Atmospheric Research 328 (2026) 108402

Contents lists available at ScienceDirect

Atmospheric Research

journal homepage: www.elsevier.com/locate/atmosres

Added value of a multi-model ensemble of convection-permitting rainfall reanalyses over Italy

Antonio Giordani *, Paolo Ruggieri *, Silvana Di Sabatino

Department of Physics and Astronomy (DIFA) "Augusto Righi", University of Bologna, Bologna, Italy

ARTICLE INFO

Keywords:
Multi-model ensemble
Convection-permitting
Regional reanalysis
Precipitation

ABSTRACT

Regional convection-permitting meteorological reanalyses substantially improve the atmospheric representation compared to convection-parameterized counterparts. This holds particularly for multi-scale driven variables such as precipitation in terms of spatial structures, intensity and frequency rates, or the timing and peak of its summer diurnal cycle. However, the simulation of convective-related phenomena is highly model-dependent, implying the inability to sample the full range of natural variability with single-model experiments. This challenge is exacerbated for km-scale simulations owing to the intrinsic chaotic nature underlying convection. Multi-model ensembles of high-resolution climate models demonstrate to reduce the simulation errors associated with individual model outputs over Europe. When applied to retrospective estimates, such ensemble approach could then offer a comprehensive, homogeneous, and optimized assessment of past atmospheric states.

This study presents the first multi-model ensemble of regional reanalyses over Italy considering four recently produced datasets to assess the added value of their joint use. These products are derived by dynamically downscaling the global reanalysis ERA5 with different numerical models: MERIDA_HRES, MOLOCH, SPHERA and VHR-REA_IT. The reference dataset for comparison is the pluviometer-based hourly analysis GRIPHO. The investigation over 2007–2016 includes the annual and seasonal variations in daily and hourly mean rainfall intensity and frequency, heavy precipitation occurrences, and their summer diurnal cycles. No single dataset systematically outperforms the others, and substantial inter-model variability is detected for summer precipitation. The ensemble improves rainfall statistical estimates compared to individual reanalyses by providing more realistic spatial patterns, enhanced skill, and reduced biases relative to observations. These findings have potential implications for downstream reanalysis applications.

1. Introduction

Severe precipitation is one of the most hazardous threats to terrestrial ecosystems, globally causing devastating impacts on the environment, socio-economic human activities, and animal welfare. The recent escalation of the associated impacts observed in Mediterranean regions (e.g. Cremonini et al., 2024), among others (e.g. Mohr et al., 2022), is attributable to the increased frequency and severity of extreme rainfall, primarily driven by anthropogenic climate change (Seneviratne et al., 2021; Caillaud et al., 2024), which is projected to further intensify by the end of century (Zittis et al., 2021). This situation prompts an ever-growing effort to enhance the understanding of these atmospheric events in order to enable the implementation of effective disaster-risk reduction and mitigation strategies (Shah et al., 2020). Deep moist convection (DMC) is a key process driving damaging severe weather including heavy precipitation, hail, flash floods, and windstorms. Convective precipitation, often resulting in rapid accumulation over localized regions associated with thunderstorms that typically last from a few minutes to several hours, is a primary contributor to the occurrence of devastating floods (e.g. Grazzini et al., 2020a; Grazzini et al., 2020b; Gimeno et al., 2022). Furthermore, convective precipitation is the predominant source of precipitation in many regions around the world, which role is continuously growing as a result of global warming (Han et al., 2016; Ye, 2018; Chernokulsky et al., 2019).

The advancement of precipitation process representation through numerical weather prediction (NWP) models has historically called for increasing refinements in atmospheric simulations. For example, limited-area regional climate models (RCMs) provide a more detailed representation of atmospheric system evolution due to their enhanced spatio-temporal resolution. Consequently, RCMs can outperform global

* Corresponding author.
E-mail addresses: antonio.giordani3@unibo.it (A. Giordani), paolo.ruggieri2@unibo.it (P. Ruggieri), silvana.disabatino@unibo.it (S. Di Sabatino).

https://doi.org/10.1016/j.atmosres.2025.108402
Received 18 April 2025; Received in revised form 4 July 2025; Accepted 3 August 2025
Available online 5 August 2025

climate models (GCMs) from which they are derived through downscaling. Indeed, many aspects of the simulations are improved when transitioning from meso-α to meso-β spatial resolutions (e.g., Torma et al., 2015), but no systematic benefits have been detected when decreasing the grid spacing from e.g. 50 to 10 km (Kotlarski et al., 2014). A substantial leap forward has been achieved when moving to the convection-permitting (CP) scale (also referred to as convection-allowing, convection-resolving, or km-scale), where NWP models employ horizontal grid spacings of only a few km (≤ 4). This allows to switch off deep convection parameterization schemes, which are major sources of errors and inaccuracies. CP models enable the explicit representation of most deep convective processes (Weisman et al., 1997), which has been shown to significantly improve the quality of the simulations, particularly of convective-related phenomena (Prein et al., 2015; Leutwyler et al., 2017). The advantages of CP models over their coarser-resolution counterparts have been detected across numerous aspects, as thoroughly reviewed by Prein et al., 2015. These advantages include: enhanced representation of precipitation intensities (Ducrocq et al., 2008; Prein et al., 2013a), improved summer diurnal cycles (Fosser et al., 2015; Brisson et al., 2016), and a reduction in intensity and frequency biases for average and extreme daily and hourly rainfalls (Berg et al., 2013; Ban et al., 2014; Pal et al., 2019). Moreover, CP models exhibit better spatial variability and finer structure concerning localized precipitation extremes (Wahl et al., 2017; Stocchi et al., 2022), effectively simulate the formation of convective self-regenerating thunderstorms (Clark et al., 2016), and capture phenomena linked to interactions with complex topography and surface heterogeneities, such as urban areas and land-sea contrasts (Weusthoff et al., 2010; Prein et al., 2013b; Kirshbaum et al., 2018). These benefits are evident also when employing high-resolution retrospective numerical datasets, such as regional reanalyses or hindcasts, to analyze past precipitation states from a CP perspective (e.g. Wahl et al., 2017; Gleeson et al., 2017).

Although CP datasets have demonstrated numerous benefits in simulating convective-related phenomena, they also possess some inherent limitations. For instance, shallow convection plays a crucial role in initiating and sustaining DMC (Holloway and Neelin, 2009), yet is not explicitly represented at CP scales and remains a sub-grid scale process that needs to be parameterized (Soares et al., 2004). This constraint could adversely affect the accurate representation and organization of convection (Teixeira et al., 2008). Consequently, CP simulations are highly-model dependent owing to both the intrinsic chaotic nature of convective processes and the numerical approximations introduced to describe them. Ensemble simulations have emerged as an effective method to take into account the uncertainty inherent in the chaotic atmospheric system by probabilistically sampling potential evolutionary paths of a simulation through initial-condition perturbations (e.g. Molteni et al., 1996). For instance, CP-model ensembles have demonstrated their ability to improve the characterization of future climatic rainfall projections (Kendon et al., 2019), enhance the skill of short-range precipitation forecasts (Ferrett et al., 2021), and provide a more accurate representation of heavy precipitation events (Klasa et al., 2018; Cerenzia et al., 2020). However, while ensembles generated from single-model experiments can effectively estimate the uncertainty related to initial conditions, they may under-represent the full spectrum of natural variability inherent in the physical processes involved. This limitation undermines the reliability of the estimates derived from individual numerical models, which are inherently biased by their specific physical assumptions (e.g. Tebaldi and Knutti, 2007; Deser et al., 2012). The absence of comprehensive sampling of the atmospheric system's internal variability is further amplified at finer spatial scales, where local interactions between the atmosphere and surface heterogeneities can exert a stronger influence (Hawkins and Sutton, 2009; Deser et al., 2014).

To address this limitation, multi-model ensembles (MMEs) – which involve the concurrent use of mulitple modeling configurations, each with its distinct physical representations – have gained increasing interest in climate and weather sciences (Sahai et al., 2021). These MMEs have demonstrated notable improvements over single-physics simulations (e.g. Greybush et al., 2017; Xu et al., 2020). Indeed, MMEs enhance the sampling of the atmosphere's internal variability, particularly in low-predictability scenarios such as extreme convective events. This consent to strengthen the robustness of NWP models outputs (e.g. Fowler et al., 2007; Wu et al., 2014), which is essential for developing effective climate adaptation and mitigation strategies. Novel applications of RCMs at the CP scale within a MME framework – previously approached from a single-model perspective – have demonstrated added value in accurately capturing high-impact precipitation occurrences. These enhancements include: improved simulations of specific and dynamically diverse severe events (Coppola et al., 2020; Capecchi, 2021; Giovannini et al., 2021), even in regions with highly complex topography (Prein et al., 2023; Collier et al., 2024), as well as advances from the Lagrangian perspective through the implementation of tracking algorithms (Müller et al., 2023); a more accurate representation of fine-scale details and a substantial reduction of the biases relative to observations, particularly when assessing changes in local-to-regional precipitation patterns under both historical and future climate scenarios (Kendon et al., 2019; Kendon et al., 2021; Pichelli et al., 2021; Kim et al., 2024), with notable improvements during the summer season (Ban et al., 2021); and an enhanced adherence to the diural cycle of precipitation (Van Lipzig et al., 2023).

However, to our knowledge, no investigations have yet been undertaken to assess the potential of the MME framework applied to a set of CP retrospective regional reanalyses. Conducting such evaluation could be valuable to determine an optimized reference of a historical period, which would serve as a robust baseline for assessing potential changes in the present and future evolution of the climate system. Indeed, CP reanalyses provide a comprehensive, multivariate and homogeneous description of past atmospheric conditions, bridging discontinuity gaps in historical observations. This capability not only advances our understanding of past climate variability (Dee et al., 2011; Hersbach et al., 2020), but also provides valuable datasets for the training of cutting-edge machine-learning-based data-driven models (e.g. Lang et al., 2024). In recent years numerous efforts have been devoted to the production of high-resolution CP regional reanalysis products for Italy (Capecchi et al., 2023; Giordani et al., 2023; Adinolfi et al., 2023; Viterbo et al., 2024). Recently, the precipitation fields derived by these products have been inter-compared among each other and with lower-resolution reanalysis datasets (Cavalleri et al., 2024b). The results highlighted the added value of CP frameworks in reproducing local-scale daily rainfall patterns, although they also revelaed a substantial increase in biases and a reduction in the inter-coherence among high-resolution reanalyses, particularly during the summer season. Hence, this study aims to synthesize these individual efforts through a MME approach to assess whether combining diverse CP reanalysis products can enhance the characterization of precipitation over Italy. Additionally, it aims to analyze the inherent inter-model variability that reflects the internal uncertainties associated with the varying physical representations involved.

The remainder of the manuscript is organized as follows: Section 2 outlines the characteristics of the regional reanalyses, the observational reference considered, and the methods adopted to construct and evaluate the performance of the MME; Section 3 presents the results of the analysis, distinguishing between annual and seasonal trends, and detailing both daily and hourly precipitation, as well as examining three significant heavy precipitation events of varying dynamical characteristics; in Section 4 we discuss the implications of these findings, while Section 5 concludes the paper with a summary of the results and proposes potential avenues for future research and applications.

2. Data and methods

This section describes the CP reanalyses included in the study, the

observative reference considered for their evaluation, and the analysis approach applied.

2.1. High-resolution reanalysis datasets over Italy

The main characteristics of the reanalysis datasets considered are summarized in Table 1. Each dataset is derived through a dynamical downscaling of the global ECMWF Reanalysis v5 (ERA5 - Hersbach et al., 2020), which is produced at the European Centre for Medium-Range Weather Forecasts (ECMWF). All individual datasets have demonstrated quantitative improvement over their common driver, ERA5, for the representation of precipitation (Capecchi et al., 2023; Giordani et al., 2023; Adinolfi et al., 2023; Viterbo et al., 2024). The spatial domains of all datasets are centered over Italy (Fig. 1a) with horizontal grid spacings ranging from 2.2 to 4 km. These resolutions allow to turn off the deep-convection parameterization schemes in the driving NWP models, hence, only shallow convection is parameterized with a common reduced mass-flux closure scheme (Tiedtke, 1989). The output fields for all datasets are generated at hourly temporal frequency. Recent inter-comparisons conducted by Cavalleri et al. (2024b) have exaxmined the daily precipitation characteristics of these products against coarser reanalyses, revealing substantial variability among them. The findings underscore the enhanced value of the CP representation at the local scale, particularly in contrast to convection-parameterizing counterparts. In the following we provide a concise overview of each dataset; for further details readers are referred to the respective scientific publications.

MERIDA_HRES: the MEteorological Reanalysis Italian DAtaset High-resolution for Renewable Energy Sources (MERIDA_HRES; Viterbo et al., 2024) is produced by Ricerca sul Sistema Energetico (RSE) as a 4-km refinement of the original MERIDA reanalysis obtained by downscaling ERA5 at a horizontal resolution of 7 km (Bonanno et al., 2019). MERIDA_HRES is driven by the NWP model Weather Research and Forecasting – Advanced Research (WRF-ARW – Skamarock et al., 2008) v3.9 over the years 1986–2022. A set of observational data is assimilated to steer the numerical simulations towards the reference atmospheric state. Particularly, a spectral nudging scheme is employed to assimilate observations related to geopotential height, temperature, and horizontal wind components, while continuous nudging is used to assimilate 2 m-temperature information. Additionally, aerosol data reconstructed from the global reanalysis dataset Modern-Era Retrospective analysis for Research and Applications, version 2 (MERRA-2 – Molod et al., 2015) are integrated into the MERIDA_HRES framework.

MOLOCH: the NWP non-hydrostatic and fully compressible model MOdello LOCale in Hybrid coordinates (MOLOCH – Malguzzi et al., 2006), maintained by the Italian InStitute of Atmospheric sciences and Climate - National Research Council (ISAC-CNR), has been considered to develop a CP hindcast at 2.5 km horizontal grid spacing by LAboratorio di Meteorologia e Modellistica Ambientale per lo sviluppo sostenibile (LAMMA – Capecchi et al., 2023). The retrospective dataset is obtained by dynamically downscaling ERA5, which involves an intermediate nesting procedure over Europe using the BOlogna Limited Area Model (BOLAM – Davolio et al., 2020) with a 7 km horizontal grid. BOLAM is then further refined over Italy to achieve the final high-resolution grid of MOLOCH for the period 1979–2024.

SPHERA: the Special Project High rEsolution ReAnalysis over Italy (SPHERA – Cerenzia et al., 2022; Giordani et al., 2023) is a regional reanalysis produced by the hydro-meteo-climate service of the Emilia Romagna region, Italy (ARPAE-SIMC) through the non-hydrostatic limited-area model COnsortium for Small-scale MOdelling (COSMO - Schättler et al., 2018) v5.05 at the CP horizontal grid spacing of approximately 2.2 km. A continuous nudging scheme is implemented to assimilate observational data of pressure, wind speed, humidity and temperature at the local scale in order to steer the model trajectories

Table 1
Main technical characteristics of the regional reanalysis datasets considered.

DATASET	MERIDA_HRES	MOLOCH	SPHERA	VHR-REA_IT
Developing institute	RSE	LAMMA	ARPAE	CMCC
Initial conditions	ERA5	ERA5/BOLAM	ERA5	ERA5
Boundary conditions	ERA5 (updated every 1 h)	ERA5 (updated every 6 h)	ERA5 (updated every 1 h)	ERA5 (updated every 3 h)
Nesting	1 step	2 step (intermediate step through BOLAM)	1 step	1 step
Spatial domain	33°N, 3°W; 52°N, 28°E	34.2°N, 2.4°E; 49.6°N, 19.9°E	35°N, 5°E; 49°N, 20°E	36°N, 5°E; 48°N, 20°E
Horizontal resolution	0.04° (~4 km), 520 × 520 grid cells	0.023° (~2.5 km), 506 × 626 grid cells	0.02° (~2.2 km), 576 × 701 grid cells	0.02° (~2.2 km), 585 × 730 grid cells
Vertical resolution	56 levels	50 levels	65 levels	50 levels
Temporal frequency	1 h	1 h	1 h	1 h
Time span	1986–2022	1979–2024	1995–2020	1989–2023
NWP model	WRF-ARW v3.9	MOLOCH	COSMO v5.05	COSMO-CLM v5.0
Data assimilation	Spectral nudging of geopotential height, temperature, wind. Observation nudging of 2 m-temperature. Assimilation of MERRA2 reanalysis aerosol data	NO	Continuous observational nudging of pressure, horizontal wind speed, humidity and temperature	NO
Microphysics scheme	5-class single-moment scheme (Thompson et al., 2008)	5-class single-moment scheme (Drofa and Malguzzi, 2004)	5-class single-moment scheme (Doms et al., 2011)	
Land-surface scheme	6-layer soil model (with 6 months of spin-up) NOAH-MP (Niu et al., 2011)	7-layer soil model (Buzzi et al., 2014)	7-layer soil model TERRA (Doms et al., 2011)	7-layer soil model TERRA (Doms et al., 2011) with TERRA-URB for urban parameterization (Wouters et al., 2016)
Boundary layer scheme	Yonsei University scheme (Hong et al., 2006)	1.5 order closure scheme (Zampieri et al., 2005)	2.5 order closure scheme (Mellor and Yamada, 1982)	1.5 order closure scheme (Mellor and Yamada, 1982)
Shallow convection scheme	Reduced mass-flux closure only for shallow convection (Tiedtke, 1989)			
Radiation scheme	Rapid radiative transfer model (Iacono et al., 2008)	δ two-stream scheme (Ritter and Geleyn, 1992) and ECMWF radiation scheme (Morcrette et al., 2008)	δ two-stream scheme (Ritter and Geleyn, 1992)	
Reference	Viterbo et al. (2024)	Capecchi et al. (2023)	Giordani et al. (2023)	Raffa et al. (2021)

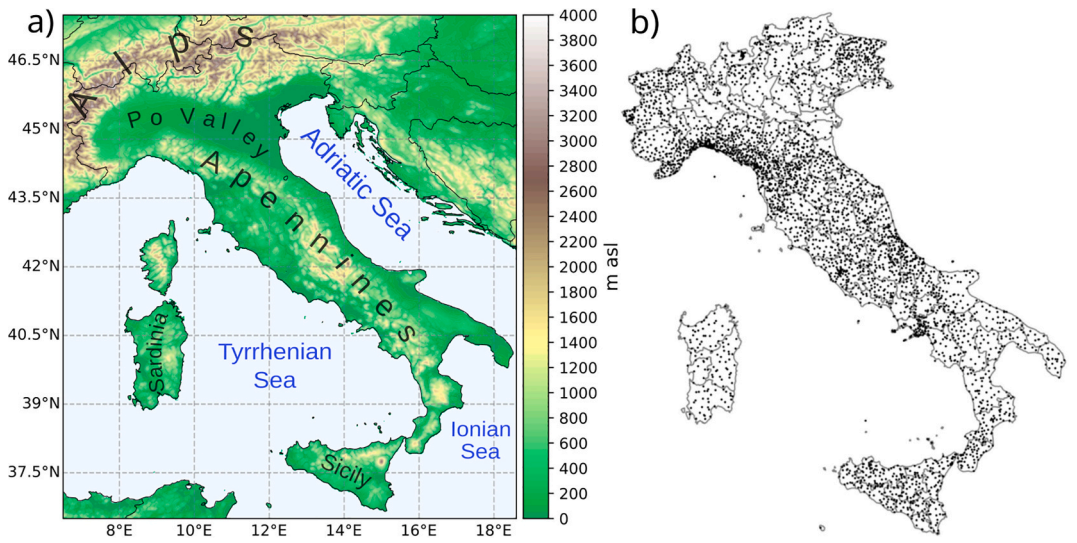

Fig. 1. a) The spatial domain and model orography. b) The distribution of the 3712 rain gauges included in GRIPHO (taken from Fantini, 2019).

towards the observed atmospheric state. SPHERA covers Italy, neighbouring countries and surrounding seas over the years 1995–2020.

VHR-REA_IT: the Very High Resolution REAnalysis for ITaly dataset (VHR-REA_IT - Raffa et al., 2021; Adinolfi et al., 2023) is a high-resolution dataset produced at the Centro euro-Mediterraneo sui Cambiamenti Climatici (CMCC) through a dynamical downscaling of ERA5 using the COSMO model in CLimate Mode (COSMO-CLM) v5.0 at 2.2 km over 1989–2023. Similarly to MOLOCH, no additional observations are assimilated at the regiornal spatial scale within VHR-REA_IT.

2.2. Observations

To assess the performance of the ensemble of regional reanalyses, the GRidded Italian Precipitation Hourly Observations (GRIPHO) dataset is considered (Fantini, 2019), which is produced by the Abdus Salam International Centre for Theoretical Physics (ICTP). GRIPHO is obtained from a statistical interpolation of over 3700 rain gauges across the Italian domain (Fig. 1b) after data checking, flagging and cleaning. Further, a validation and comparison with other precipitation observational products has also been performed (Fantini, 2019). The resulting rain-gauge analysis offers an estimate of precipitation over Italy at hourly frequency on a 3-km grid, covering the period 2001–2016. While the GRIPHO dataset boasts high spatio-temporal resolution, it is essential to acknowledge certain limitations when interpreting rainfall observations from in-situ instruments (Prein and Gobiet, 2017). These limitations include the underestimation of precipitation intensity in regions with sparse or heterogeneous sensors distribution (for instance in montainous regions – Crespi et al., 2018). Additionally, systematic under-catching may occur due to wind-induced drifting of hydrometeors (La Barbera et al., 2002), as well as potential losses from wetting and evaporation (Frei et al., 2003). Further, the interpolation of data from sparse sensor networks onto a regular grid - a necessary procedure for homogenizing spatial information - can introduce further discrepancies between interpolated values and the actual rainfall state. These discrepancies may manifest as underestimations of peak and localized rainfall intensities owing to spatial smoothing, as well as overestimations of lower intensities resulting from the spread of moist fields into drier regions (Isotta et al., 2014). Previous research has indicated that undercatching by rain gauges can lead to substantial underestimations of rainfall, potentially ranging from 4 to 50 % (Frei et al., 2003). Accordingly, to account for potential observational uncertainties, the following analysis considers relative biases in rainfall measurements between numerical datasets and observations to be acceptable within a range of −5 % to +25 % (Frei et al., 2003; Ban et al., 2021).

2.3. Analysis and statistical indices

This study presents a comprehensive statistical analysis of precipitation patterns, considering both individual datasets and their ensemble aggregations over the common period 2007–2016. The methodology adopted for the statistical assessment mostly builds on the approaches of Ban et al. (2021) and Pichelli et al. (2021), who investigated various aspects of rainfall within a MME framework of CP RCMs over Europe, providing a comprehensive evaluation of their performance. We employ a set of statistical indices evaluating diverse characteristics of rainfall estimates at both daily and hourly resolutions (Table 2). The analysis is conducted by considering annual and seasonal aggregations separating among: spring (March–April–May; MAM), summer (June–July–August; JJA), fall (September–October–November; SON), and winter (December–January–February; DJF). To take into account the influence of drizzle and very light rain on the statistical distributions, we separately consider wet days (or wet hours) as those with accumulated precipitation exceeding 1 mm per day (or 0.1 mm per hour). Additionally, to explore the characteristics of heavy precipitation events, we examine indices based on the 99th percentile for daily precipitation and the 99.9th percentile for hourly precipitation across the complete datasets, which includes both wet and non-wet days and hours following Schär et al., 2016. A pre-processing step is employed across all numerical and observational datasets to homogenize the representativeness of their outputs, ensuring comparability of results. This involves reprojection onto a common regular grid with horizontal resolution of 3 km, achieved through a conservative remapping method (Diaconescu et al., 2015). The selected grid minimizes deviations from the reference dataset, which has a comparable native resolution, while also accomodating the varying resolutions of the individual datasets, which range from 2.2 to 4.0 km. An observational mask is applied to retain only those grid points

Table 2
Statistical indices employed in the analysis. A wet day (hour) is defined as a day (hour) with precipitation $\geq$1 mm • d^{-1} ($\geq$ 0.1 mm • h^{-1}). Heavy daily (hourly) precipitation is defined as the percentile 99th (99.9th) of the distribution.

Index	Symbol	Units
Mean daily precipitation	$\overline{dd}$	mm • d^{-1}
Wet day/hour intensity	$\overline{dd}_{int}$ / hh_{int}	mm • d^{-1} / mm • h^{-1}
Wet day/hour frequency	dd_{freq} / hh_{freq}	fraction
Heavy daily/hourly precipitation	dd_{p99} / $hh_{p99.9}$	mm • d^{-1} / mm • h^{-1}

where GRIPHO values are present, thus focusing exclusively on locations over land within the Italian territory. This process yields an average of 36,458 valid grid points. Subsequently, the spatio-temporal distributions of the four numerical datasets are then aggregated through concatenation to generate the MME estimate.

The performance of individual datasets and ensemble-derived estimates for the statistical indices listed in Table 2 is assessed considering a comprehensive suite of skill-score metrics, as detailed in Table 3, to enable a thorough evaluation of various precipitation characteristics. Three skill scores - namely, spatial correlation coefficient (ρ_{spat}), spatial variability (*SpatVar),* and centered and normalized root mean squared error (*CRMSE*) - can be summarized in the Taylor diagram due to their inherent geometric relationships (Taylor, 2001). Indeed, through the Law of Cosines it is possible to write:

$$CRMSE^2 = \sigma_{mod}^2 + \sigma_{obs}^2 - 2\sigma_{mod}\sigma_{obs}\rho_{spat}$$

where σ_{mod} and σ_{obs} represent the spatial standard deviations of the modeled (i.e. reanalysis) and observed precipitation fields, respectively. The Taylor diagram facilitates a visual assessment of the similarity between numerical datasets and observational data, enabling the identification of deviations in the modeled precipitation fields from the ideal state (having $\rho_{spat} = 1$, $SpatVar = 1$ and $CRMSE = 0$). Additionally, we consider the Equitable Threat Score (ETS) for quantifying the skill of reanalyses in predicting precipitation exceedances for a set of thresholds (Schaefer, 1990). The ETS is a categorical verification metric that accounts for hits that could occur by random chance and is defined as:

$$ETS = \frac{H - H_r}{H + F + M - H_r} \text{ with } H_r = \frac{(H+F)\cdot(H+M)}{N}$$

where H is the number of hits (correct forecasts of event occurrence), F is the number of false alarms (forecasted events that did not occur), M is the number of misses (events that occurred but were not forecasted), and H_r is the number of hits expected by chance given the total number of forecasts N. The ETS ranges from $-\frac{1}{3}$ to 1, where 1 indicates a perfect forecast, 0 corresponds to no skill beyond random chance, and negative values indicate worse-than-random forecasts. By adjusting for chance agreement, ETS provides a more equitable assessment of forecast quality than the traditional Threat Score, especially for rare events such as heavy precipitation. The diurnal cycle of summer precipitation is also analyzed, which is a critical aspect largely influenced by the variations in convective activity throughout the day. To gain insights into the impact of topographical diversity on precipitation distribution in Italy, the daily cycles are calculated separating the grid points by altitude: plains (0–300 m above sea level, asl.), hills (300–600 m asl.), and mountains (> 600 m asl.). Additional investigations focused on case studies of high-impact precipitation events occurring in different seasons are included. For these events the Contiguous Rain Area (CRA) analysis is considered (Ebert and McBride, 2000). The CRA is an object-oriented method that aims at objectively verify distinct spatial entities of rainfall fields, where an entity is anything that can be defined by a closed contour. For each entity identified in the reanalysis and observed precipitation fields, the CRA verification employs pattern matching techniques to quantify the mean location error of the centroids features, the mismatches of their areal extents, as well as the mean rainfall intensity errors. To prevent duplicate matches among reanalyses and observations, the Hungarian algorithm is implemented to assure one-to-one features matching (e.g., Raut et al., 2021). In order to select only precipitation features associated with heavy rainfall, a mask based on the exceedance of the 75th percentile of the aggregated GRIPHO fields over the event is applied to the spatial distribution of every dataset. Furthermore, to avoid possible matches among excessively distant and unrelated spatial features, a maximum distance threshold of 30 km between the centroids of reanalyses and GRIPHO entities is applied.

3. Results

In this section we present the results of the MME analysis, considering seasonal aggregations, the summer daily cycle of precipitation, and their annual characteristics. Further, a detailed examination of three dynamically-diversified high-impact precipitation events is provided.

3.1. Seasonal analysis

The seasonal inter-MME variability of the relative bias with the observed precipitation is shown in Fig. 2, which employs box-plots to depict the distribution of deviations from observed values across the set of rainfall indices. Each box-plot encompasses the biases associated with four individual datasets, while the ensemble's overall deviations are represented by magenta solid dots. Across all seasons, with the exception of JJA, the distribution of biases exhibits a compact spread, generally embedded within the acceptable bias range of −5 % to +25 % (highlighted area in sea green). This suggests a lower magnitude and variability of deviations from observed precipitation. In contrast, during JJA, there is a notable increase in both the spread and intensity of the biases towards excessively wet conditions, with mean overestimations reaching or exceeding 50 % for indices associated with precipitation intensity ($\overline{dd}$, dd_{p99}, hh_{int}, $hh_{p99.9}$), as reported in the associated literature (Adinolfi et al., 2023; Capecchi et al., 2023; Giordani et al., 2023; Viterbo et al., 2024; Cavalleri et al., 2024b). The ensemble aggregations primarily yield biases concentrated in the central portions of the distributions represented in the box plots, specifically within the interquartile range (i.e., between the 25th and 75th percentiles), mitigating the wet biases associated with single-reanalysis estimates. Exceptions to this trend are noted for extreme precipitation indices, which exhibit contrasting behaviors. For heavy daily precipitation (dd_{p99}), the ensemble reduces the bias across all seasons, resulting in an almost unbiased estimate for JJA and a dry bias of approximately −10 % for other seasons. Conversely, for heavy hourly precipitation ($hh_{p99.9}$), the ensemble results in an intensification of the wet bias, exceeding the 75th percentile of the distributions for all seasons when compared to most individual datasets. These contrasting findings are likely attributable to a smoothing effect that takes place during the ensemble aggregation of the distribution tails of single datasets associated with extreme precipitation. Fig. 3 reports the seasonal quantile-quantile plots comparing the reanalyses with GRIPHO for dd_{p99} and $hh_{p99.9}$, providing additional insights into this aspect. The ensemble aggregation tends to systematically

Table 3
Skill-score metrics considered to evaluate the performance of precipitation estimates.

Skill score	Symbol	Description
Spatial correlation	ρ_{spat}	Spatial correlation between reanalysis datasets and observations across all grid points
Spatial variability	*SpatVar*	Ratio between the spatial standard deviations of reanalysis datasets and observations across all grid points ($\frac{\sigma_{mod}}{\sigma_{obs}}$)
Centered and normalized root mean-squared error	*CRMSE*	Area-weighted mean of the centered root-mean squared error between reanalysis datasets and observations, normalized with σ_{obs}
Relative bias		Relative difference $\frac{model - obs}{obs}$ of spatially averaged/distributed rainfall indices
Equitable Threat Score	*ETS*	Measure of the skill of reanalysis in predicting precipitation exceeding a certain threshold while accounting for hits that could occur by random chance

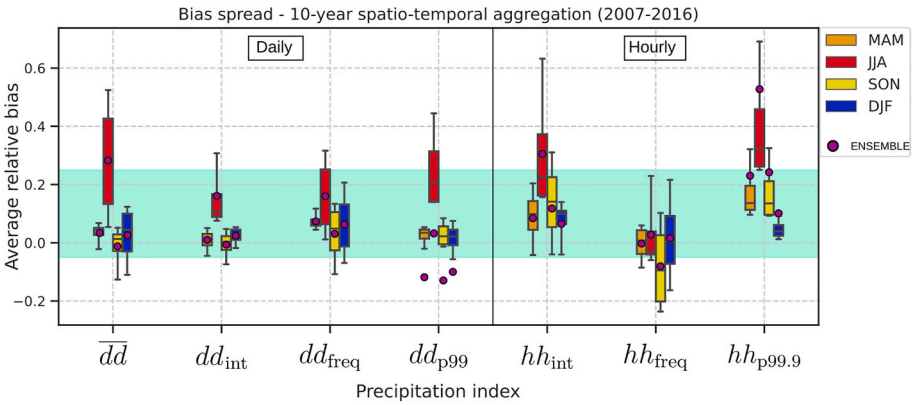

Fig. 2. Box-plots of the seasonal average relative bias spread compared to GRIPHO observations for the precipitation indices listed in Table 2. Data are aggregated over the entire spatio-temporal domain and categorized by season: MAM (orange), JJA (red), SON (yellow), and DJF (blue). The boxes represent the distribution of bias including the four single datasets, while the magenta solid dots indicate the corresponding ensemble aggregations. The sea-green shaded area highlights the acceptable uncertainty range due to rain-gauge undercatch, as detailed in Section 2.2. (For interpretation of the references to colour in this figure legend, the reader is referred to the web version of this article.)

and increasingly underestimate daily precipitation extreme intensities compared to single reanalyses especially in JJA and SON (panels b-c). In contrast, for hourly extremes (panels e-h), SPHERA exhibits the largest overestimations, which substantially contribute to the ensemble deviation from the GRIPHO reference. The spatial distributions of dd_{p99} and $hh_{p99.9}$ for JJA, derived from the four individual reanalyses and their ensemble aggregation (Figs. A1 and A2, respectively), along with the corresponding Taylor diagrams (Fig. A3) and relative bias maps (Fig. A5 and A6 respectively), provide a visual assessment of the smoothing effect on extreme rainfall estimates.

To assess the performance in reproducing seasonal rainfall intensities, the ETS skill score is analyzed in Fig. 4 for increasing rainfall exceedance thresholds for daily and hourly estimates during JJA and DJF (corresponding results for MAM and SON are presented in Fig. A4). The ensemble aggregation (purple dotted-lines) consistently exhibits the highest skill both for daily and hourly estimates across all seasons, until, together with all individual-dataset curves, it tends to converge towards low skill values (i.e. $\gtrsim$ 7.5 mm/h and $\gtrsim$ 80 mm/d). This indicates the ensemble's systematically superior ability to accurately identify observed precipitation occurrences while reducing the number of false alarms and misses relative to individual reanalyses. Moreover, the ensemble's skill improves most notably over individual reanalyses in summer, a season characterized by higher uncertainty in simulating convective precipitation, whereas individual reanalysis skills tend to be similar and lower.

In light of the peculiar characteristics observed during the summer months and the increasing interest in accurately representing high-impact warm-season convective rainfall, we provide a comprehensive analysis of the spatial distribution of precipitation during JJA. Fig. 5 illustrates the JJA mean daily precipitation ($\overline{dd}$) spatial distribution averaged across the ten years included in this study. The four reanalysis datasets exhibit consistent spatial patterns in the mean summer daily

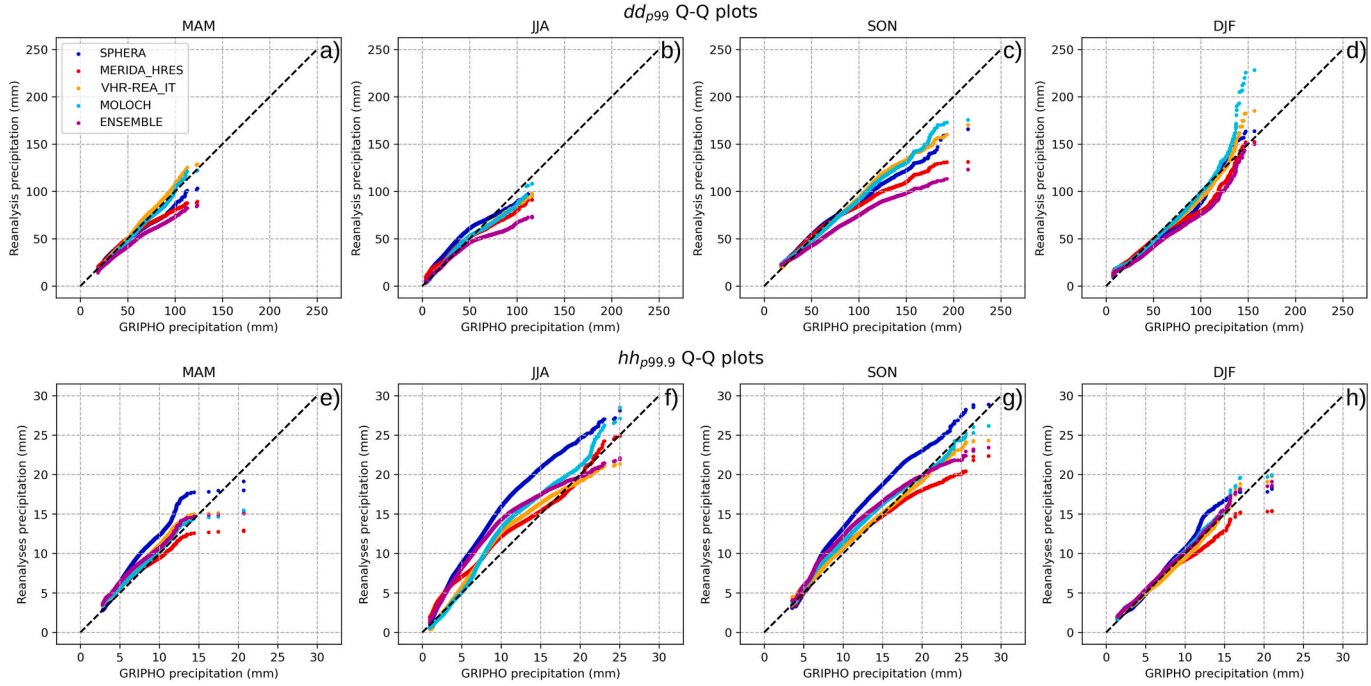

Fig. 3. Seasonal quantile-quantile plots of dd_{p99} (upper row) and $hh_{p99.9}$ (lower row) over 2007–2016 of SPHERA (blue), MERIDA_HRES (red), VHR-REA_IT (orange), MOLOCH (cyan), and their ensemble aggregation (magenta) against GRIPHO distributions. MAM (a-e), JJA (b-f), SON (c-g), and DJF (d-h). (For interpretation of the references to colour in this figure legend, the reader is referred to the web version of this article.)

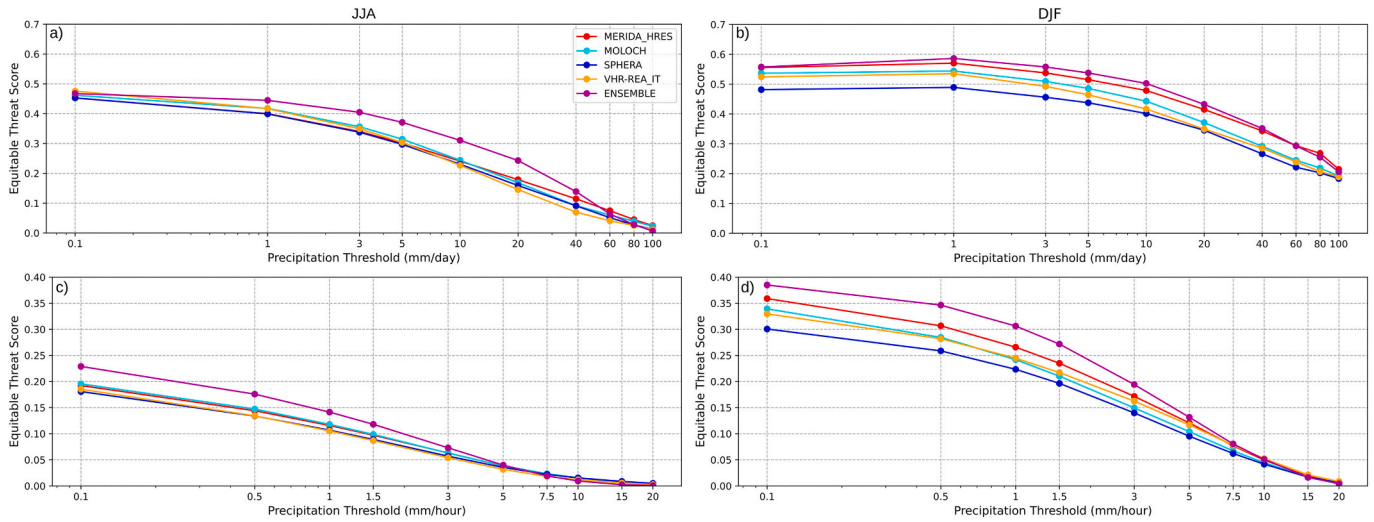

Fig. 4. Seasonal ETS skill scores for a set of daily (upper row) and hourly (lower row) precipitation exceedance thresholds, for JJA (a-c) and DJF (b-d). MERIDA_HRES (red), MOLOCH (cyan), SPHERA (blue), VHR-REA_IT (orange) and their ENSEMBLE aggregation (magenta). (For interpretation of the references to colour in this figure legend, the reader is referred to the web version of this article.)

rainfall estimates, with the Alpine region demonstrating the highest values, including peaks exceeding 6 mm d^{-1}. Additionally, localized precipitation maxima are identified throughout the Apennines, particularly in northwestern Italy, the central peninsula, and the central Calabria region near the Sila plateau. Conversely, the driest areas, characterized by average accumulations of less than 1 mm d^{-1}, include the main islands (Sardinia and Sicily), southern Apulia, and sections along the Tyrrhenian coast. MERIDA_HRES and MOLOCH exhibit comparable spatial distributions; however, MOLOCH is characterized by sharper precipitation peaks, particularly in regions of complex topography. SPHERA and VHR-REA_IT, both based on the COSMO model, demonstrate substantially different characteristics. SPHERA shows generally increased precipitation intensities over the northern plains, particularly the Po Valley, although producing less extreme peaks. Convesely, VHR-REA_IT notably produces the highest average precipitation amounts in the Alps, with accumulations exceeding 8.5 mm d^{-1} in north-Eastern Italy, while mitigating the precipitation intensity over the plains. The ensemble composite is found to have the most adherent

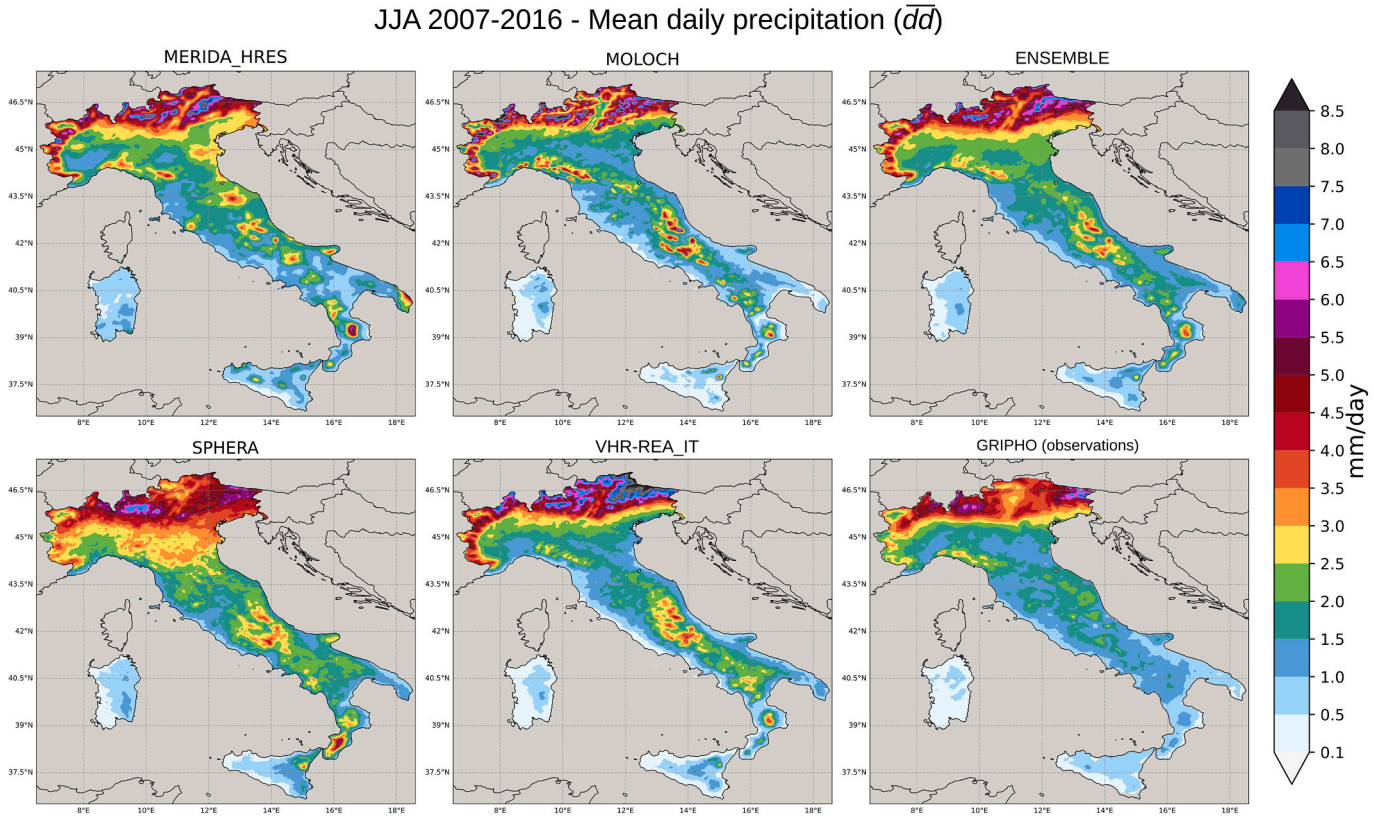

Fig. 5. Spatial distributions of $\overline{dd}$ during JJA averaged over 2007–2016. The four reanalyses estimates (left and central columns), their ensemble aggregation, and the GRIPHO observational reference (right column).

spatial structure with GRIPHO, as demonstrated by both visual assessments and quantitave mesaures. Indeed, the Taylor diagram (Fig. 6) indicates that the ensemble yields the lowest deviations from the reference state having the highest correlation coefficient (0.92), the lowest *CRMSE* (0.44), and a comparable *SpatVar* of 1.11 relative to individual datasets.

The spatial characteristics of the relative bias of daily mean precipitation during summer, as assessed against GRIPHO, are illustrated in Fig. 7. Distinct bias structures are revealed contingent upon the dataset employed. Specifically, MERIDA_HRES and MOLOCH exhibit comparable deviations, with both displaying pronounced wet biases over southern Italy and the major islands; however, MOLOCH results in drier estimates over northeastern Italy, the Tyrrhenian coast, the Apulian peninsula and Sicily. On the other hand, SPHERA and VHR-REA_IT produce a peculiar complementary spatial distribution of the bias in north-central Italy. SPHERA demonstrates an almost uniform wet bias over the Po Valley while aligning closely with observational data over the Alps. Conversely, VHR-REA_IT mitigates overestimations over the plains, albeit at the expense of exacerbating excessively wet conditions across the Alpine region - particularly in the northeastern areas - and yielding drier estimates along the western coastal regions. The ensemble composite reveals an overall reduction in bias deviation from GRIPHO, except in regions where (almost) all datasets consistently overestimate, specifically in southern Apulia, Calabria, and southern Sardinia. This improvement is quantitatively assessed via the percentage *F* of grid points exhibiting an acceptable bias, with the 4-reanalysis aggregation achieving 39.8 %, while each individual dataset registers a percentage $\leq$ 31.6 %.

3.2. Summer daily cycle

Summer precipitation in Italy is predominantly driven by deep-moist convection, which results in sub-daily rainfall variations largely governed by the diurnal cycles of lower boundary layer heating and the associated convective processes. Consequently, CP datasets are expected

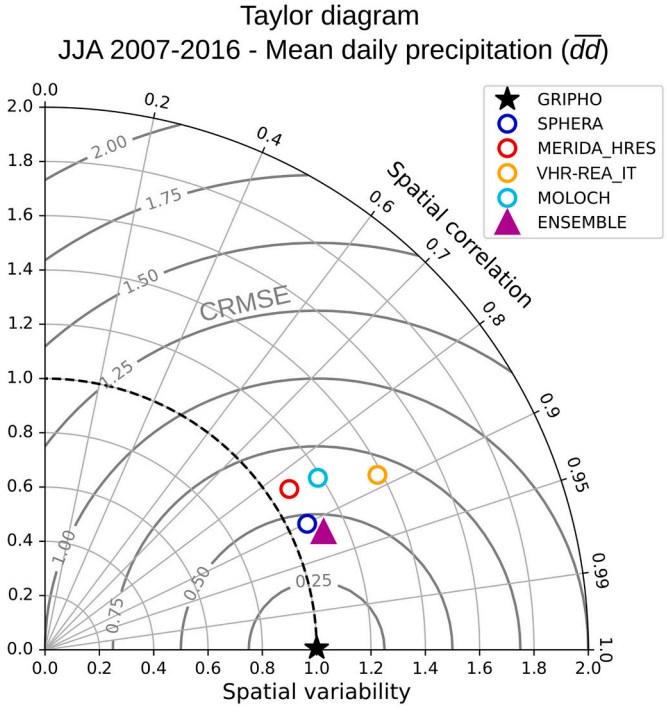

Fig. 6. Taylor diagram for the spatial distributions of $\overline{dd}$ reported in Fig. 5. GRIPHO is indicated by a solid black star, the individual reanalyses with unfilled coloured circles, and the ensemble estimate with a solid magenta triangle. (For interpretation of the references to colour in this figure legend, the reader is referred to the web version of this article.)

to capture these dynamic characteristics effectively. Fig. 8 reports the average diurnal cycles of precipitation in JJA, differentiated by plain, hill and mountain regions based on the altitude of the grid points (i.e. in the ranges of 0–300 m asl, 300–600 m asl, and > 600 m asl respectively). A diurnal signal is evident across all datasets and altitudes, exhibiting enhanced variability towards the precipitation peak observed at 15 UTC. This peak is found to be slightly anticipated of 1–2 h according to reanalyses estimates. Furthermore, there is a general trend of increasing amplitude of the diurnal cycle with altitude, attributable to the topographic amplification of precipitation characterizing the Italian region (e.g., Napoli et al., 2019). Notably, larger overestimations of the observed cycle occur in mountainous areas, which may be partially ascribed to the inherent inaccuracies of the reference state in regions with complex topography.

3.3. Annual analysis

To conduct a comprehensive evaluation of precipitation characteristics in the Italian region, an aggregation of the statistical indices based on annual data averaged over the 10-year period is included. Fig. 9 shows the heat tables of the three performance metrics included in the Taylor diagram, as listed in Table 3, considering six of the statistical indices outlined in Table 2. These metrics are examined for each individual dataset and for their ensemble aggregation. Notably, the resulting ensemble estimates tend to maximize the spatial correlation with the observations (Fig. 9a) across nearly all indices, and contributes to minimize the *CRMSE* (Fig. 9c), to a lesser extent. The analysis reveals a certain degree of variability among the performance of the four reanalyses, with a general trend indicating superior skill in daily precipitation estimates compared to hourly estimates – particularly for metrics pertaining to intensity and extreme precipitation. This discrepancy likely arises from the inherent challenges of accurately capturing rainfall at higher temporal frequency. Regarding *SpatVar* (Fig. 9b), the MME aggregation yields performances that are intermediate between those of the individual datasets, with the exception of heavy hourly precipitation ($hh_{p99.9}$), for which a reduced spatial variability is detected compared to almost all single reanalysis counterparts.

3.4. Case studies

This section examines specific events linked to high-impact precipitation occurrences to assess the performance and the potential benefits of the MME. The aim is to broaden the statistical evaluation presented thus far by incorporating the perspective of observed extreme rainfall events. Three distinct cases are considered, each associated with different dynamical forcings: 1) an intense Mediterranean cyclone that produced prolonged and persistent precipitation in central Italy during the fall season and severe impacts over extended areas (Section 3.4.1), 2) an outbreak of multiple convective storms in northeastern Italy occurred at the end of the summer season resulting in flash flooding and strong hailstorms (Section 3.4.2), and 3) a deepening of an Atlantic trough which promoted orographic precipitation over the northern Apennines in winter (Section 3.4.3). Therefore, evaluating the performance of the MME for these events of varying nature is crucial for assessing the potential benefits of improving the representation of high-impact weather occurrences.

3.4.1. Flood in central Italy due to Mediterranean cyclone (10–13 November 2013)

Beginning on the 9th of November 2013, the progressive deepening of a synoptic-scale trough over Europe led to the isolation of a cut-off low pressure system associated with a Mediterranean cyclone. Fig. 10a shows the minimum in the mean sea level pressure situated over the Thyrrenean Sea, along with the corresponding counter-clockwise rotation of the 10-m wind speed field as derived from ERA5 reanalysis for the 11th of November at 11 UTC. This large-scale atmospheric forcing

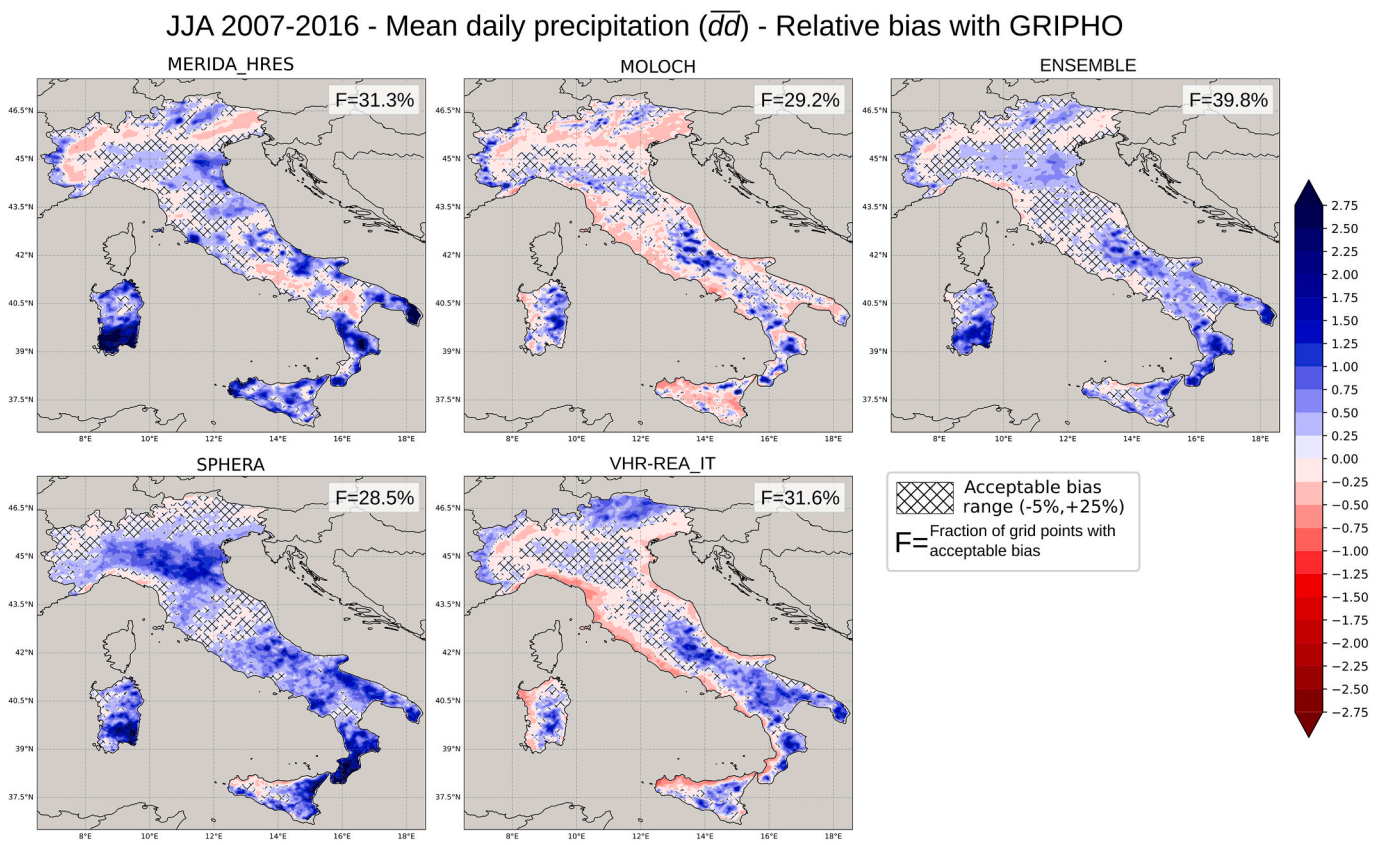

Fig. 7. Spatial distributions of relative bias with GRIPHO for $\overline{dd}$ during JJA, averaged over 2007–2016, as shown in Fig. 5. Grid points exhibiting an acceptable bias (ranging from −5 % to +25 %) are shadowed with a double hatching. Additionally, the percentage *F* of grid points falling within this acceptable range is provided for every field.

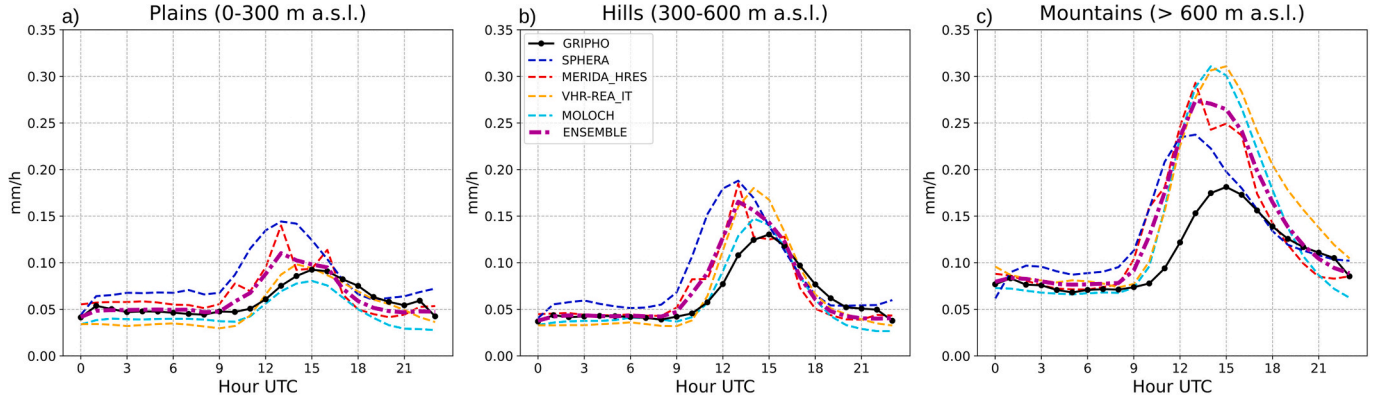

Fig. 8. Diurnal cycle of precipitation in JJA, averaged over 2007–2016, for GRIPHO (in dotted solid black lines), the four datasets MERIDA_HRES (red dashed lines), MOLOCH (cyan dashed lines), SPHERA (blue dashed lines), and VHR-REA_IT (orange dashed lines), and the ensemble mean (in magenta bold dashed-dotted lines). The precipitation distributions are separated by topograhpy among: a) plains, b) hills, and c) mountains. (For interpretation of the references to colour in this figure legend, the reader is referred to the web version of this article.)

induced the northwestward advection of humid air masses from the southeastern Mediterranean and the Balkan region, resulting in intense wind gusts and numerous storm surges over the Adriatic coastline. Furthermore, these conditions induced persistent precipitation across vast areas of central Italy as the humid air masses impinged over the Apennine mountain range (ARPAE, 2013). The impact of these events was exacerbated by an anticyclonic blocking pattern over Eastern Europe, which hindered the eastward progression of the cyclonic circulation, thereby extending the duration of favorable conditions for continued precipitation in the region. This resulted in extensive flooding, coastal erosion, landslides, and two reported fatalities (Regione Marche, 2013).

The accumulated precipitation field during the four-day event, derived from the four datasets, their ensemble composite, and GRIPHO observations, is illustrated in Fig. 11. All datasets reveal a coherent spatial structure in the rainfall distribution, with significant peaks exceeding 300 mm located in the inland regions near the Apennines mountain chain, aligning closely with observed data. Consequently, the ensemble average retains an adherent spatial structure with the observations, which is further supported by the associated Taylor diagram

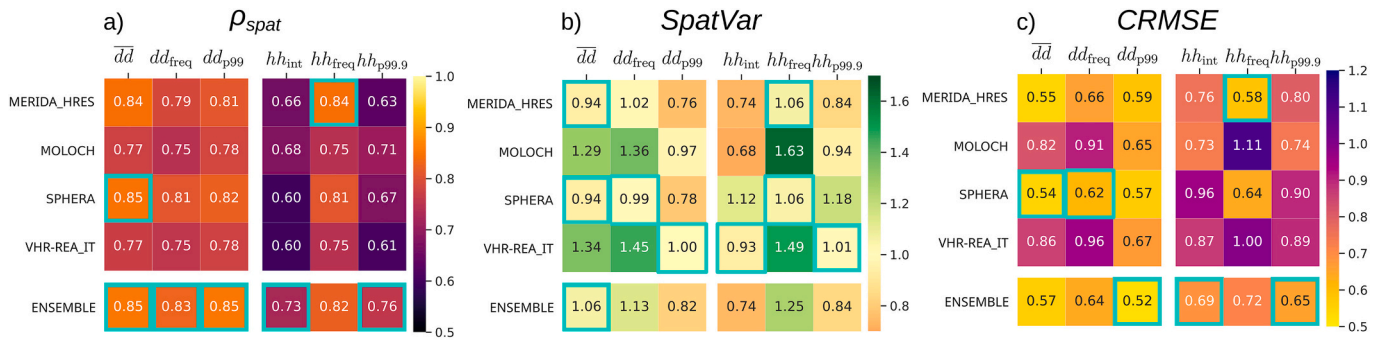

Fig. 9. Heat tables showcasing the performance evaluation of various precipitation indices (as detailed in Table 2) across three metrics (Table 3) against the GRIPHO dataset. The metrics examined are: a) spatial correlation, b) spatial variability, and c) centered and normalized root mean square error. The analysis include the four individual datasets and their ensemble aggregation, arranged in rows, while the indices are represented in the columns. The evaluation is conducted over the whole Italian domain over 2007–2016. Deviations from optimal performance (i.e., $\rho_{spat} = 1$, $SpatVar = 1$, $CRMSE = 0$) are illustrated using different colour codings, where lighter colors indicate better performance. The best-performing scores among the datasets for each metric and index are highlighted with sea-green frames. (For interpretation of the references to colour in this figure legend, the reader is referred to the web version of this article.)

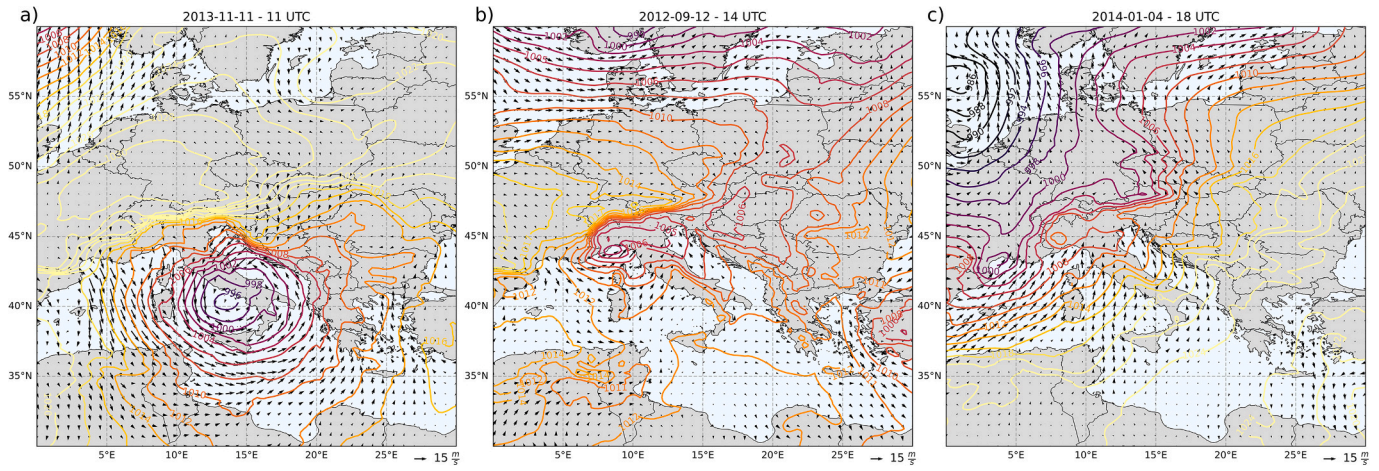

Fig. 10. Mean sea level pressure (MSLP) field, depicted with color contours, overlaid on the 10-m wind speed field derived from ERA5 reanalysis for: a) November 11, 2013, at 11 UTC, b) September 12, 2012, at 14 UTC, and c) January 4, 2014, at 18 UTC.

(Fig. 12a). The differences among the individual datasets are relatively minor, yet their ensemble aggregation demonstrates superior performance, enhancing the spatial correlation coefficient to 0.93, reducing the *CRMSE* to 0.37, and yielding a comparable *SpatVar* of 0.86. Furthermore, with respect to the CRA spatial metrics (Fig. 13a), the ensemble provides the best-performing estimates in terms of the lowest centroid distance with the observed field, a similar and slightly better rainfall intensity error compared to individual datasets, while its performance in areal extension mismatch ranks second. The added value of the MME aggregation is evident also in the temporal evolution of the event (Fig. 14), which reports hourly accumulated precipitation series recorded at the rain gauge located in the city of Rubbiano (indicated by a red star in Fig. 11, panel GRIPHO). To facilitate a point-to-point comparison, bilinear interpolation is applied to the reanalysis fields based on the station location. By the end of November 13th, the observed accumulated precipitation reached approximately 300 mm, with the most significant and rapid increase occurring on November 11th. This trend is captured by all datasets, although some either underestimated (as shown by SPHERA and VHR-REA_IT) or overestimated (as indicated by MOLOCH) the final total up to approximately 30 %. Notably, the ensemble average yields one of the most adherent curves to the observed counterpart (represented by the magenta dash-dotted line in Fig. 14), reflecting its capability to enhance the reconstruction of the temporal evolution of the event.

3.4.2. *Severe convective storms outbreak (12 September 2012)*

On the 11th September 2012 the incursion of a large-scale cold front, associated with a deep north Atlantic trough, disrupted the prolonged anticyclonic conditions that had dominated central Europe throughout the warm season. The synoptic configuration on 12 September (Fig. 10b) highlights a weaker large-scale forcing compared to the event described in Section 3.4.1, and is characterized by a shallow low-pressure region over the Po valley and the Genoa gulf, which sustains northeastward air advection over north-Eastern Italy. This advected influx initiated the destabilization of the lower troposphere, subsequently triggering the development of multiple severe convective storms in the northeastern regions on 12 September (Kerkmann et al., 2012; Ferretti et al., 2014; Manzato et al., 2015). The thunderstorms produced daily rainfall accumulations with localized recorded totals of up to 149 mm, and extended areas within the Friuli Venezia Giulia region experiencing precipitation exceeding 70 mm (Fig. 15, panel GRIPHO).

The individual dataset representations of the event (Fig. 15) exhibit considerable variability in both the magnitude and spatial distribution of the highest precipitation peaks. For instance, MERIDA_HRES predicts

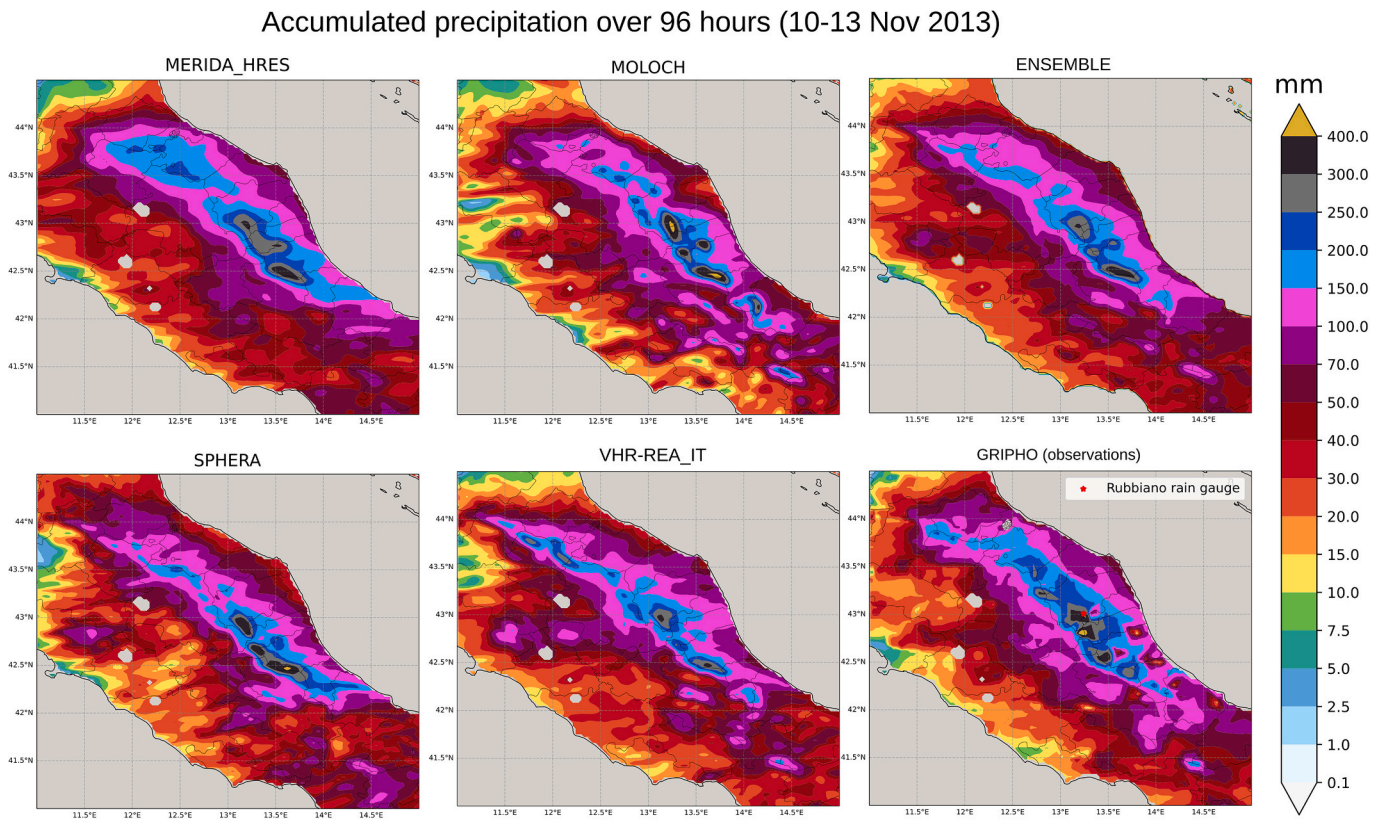

Fig. 11. Same as Fig. 5 but for the accumulated precipitation over 10–13 November 2013 over central Italy. In the sub-panel GRIPHO is highlighted the location of the rain gauge in the city of Rubbiano, marked with a red star, which recorded one of the highest rainfall accumulations during the event. The temporal series of this gauge is analyzed in Fig. 14. (For interpretation of the references to colour in this figure legend, the reader is referred to the web version of this article.)

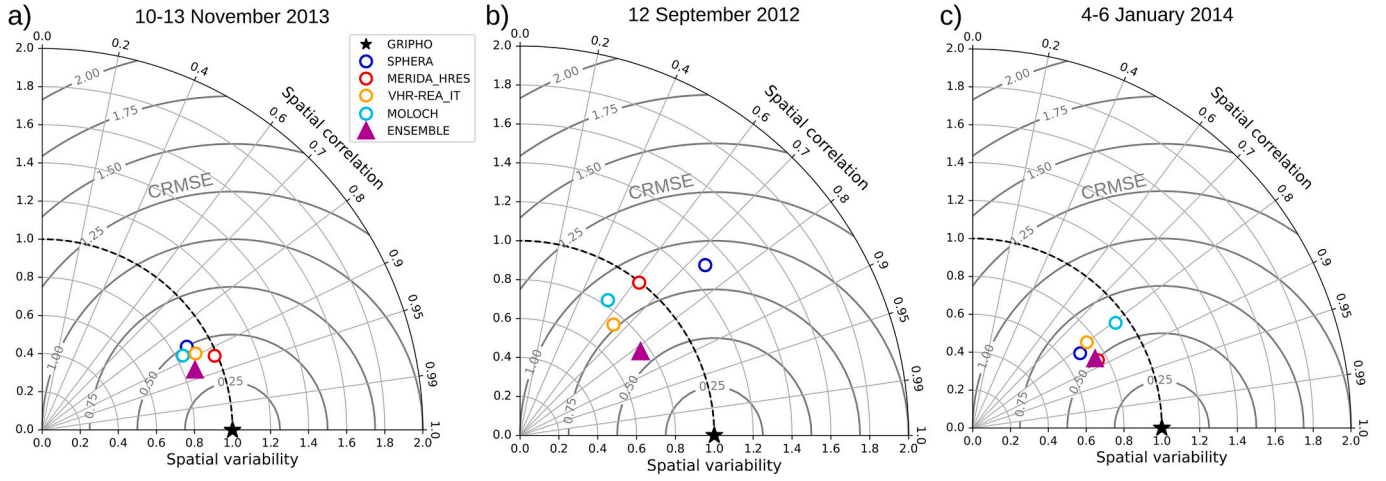

Fig. 12. Same as Fig. 6 but: a) for the spatial distributions of Fig. 9, b) for the spatial distributions of Fig. 12, c) for the spatial distributions of Fig. 16.

substantial precipitation amounts >100 mm over inland northern areas of the region, while SPHERA estimates accumulations exceeding 150 mm near the southeastern coast. In contrast, MOLOCH and VHR-REA_IT suggest more localized rainfall peaks concentrated in the vicinity of the northeastern Alps. As a result, the MME aggregation yields a more homogenized precipitation field, characterized by lower peak values (96 mm), and a notably reduced spatial variability (*SpatVar* = 0.76 in Fig. 12b), which is comparable to that of VHR-REA_IT. Despite this smoothing effect, the ensemble mean closely resembles the observed spatial patterns in GRIPHO, as quantitatively evidenced by the highest correlation coefficient (0.82) and the lowest *CRMSE* score (0.57) compared to all individual reanalysis products. A good MME performance is obtained also according to CRA metrics (Fig. 13b). Although MERIDA_HRES achieves the best scores across all the three metrics – particularly for areal extension and centroid distance, where it clearly outperforms the other products – the ensemble aggregation ranks second in all cases, highlighting its ability in capturing the spatial distribution of observed rainfall.

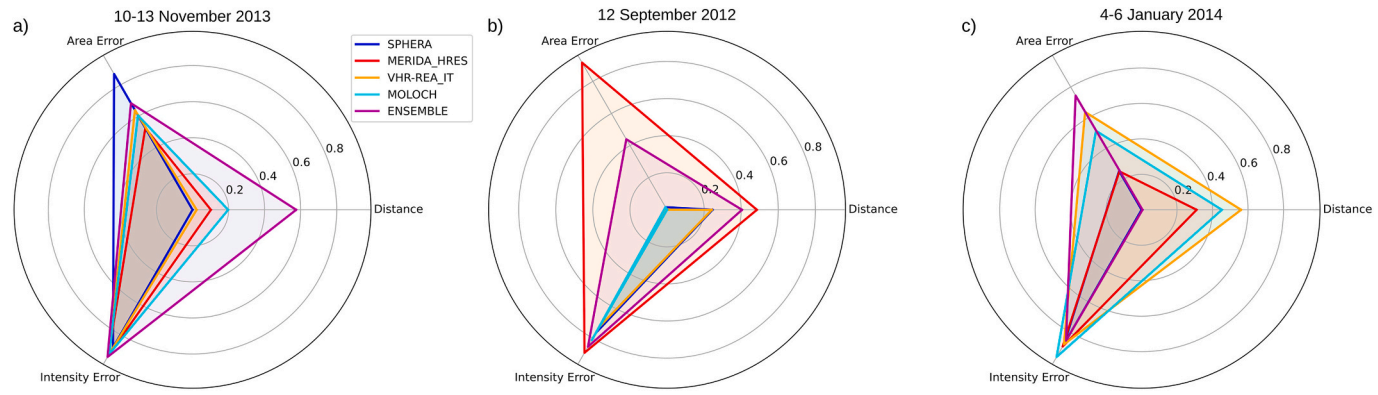

Fig. 13. Radar plots of CRA verification metrics for the three precipitation events considered: a) 10–13 November 2013, b) 12 Septeber 2012, c) 4–6 January 2014. The metrics refer to: "Distance" the distance (in km) between matched CRA spatial centroids between reanalyses and GRIPHO, normalized with the maximum detected distance among the datasets, "Area error" the relative error in CRA object spatial extension, and "Intensity error" the relative error in CRA mean intensity. The closer the scores are to 1 the more the spatial features resemble those of GRIPHO. The metrics are calculated for precipitation fields exceeding the 75th percentile values of observed distributions of Figs. 11, 15 and 16 for the three events, respectively, and considering a common maximum distance threshold of 30 km between reanalysis and GRIPHO detected spatial structures.

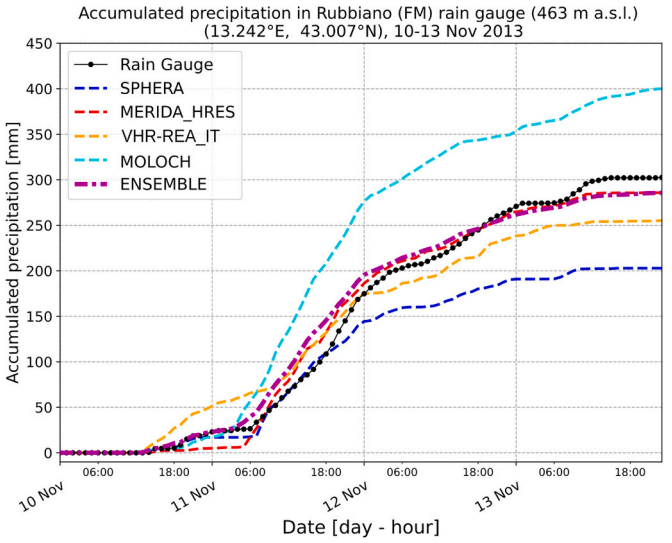

Fig. 14. Accumulated precipitation for the period 10–13 November 2013, at the Rubbiano rain gauge (indicated by a red star in Fig. 10). The observed data are represented by the solid and dotted black line, individual reanalysis estimates are reported for SPHERA (blue dashed line), MERIDA_HRES (red dashed line), VHR-REA_IT (orange dashed line), MOLOCH (light-blue dashed line), and their ensemble mean (magenta dash-dotted line).
(For interpretation of the references to colour in this figure legend, the reader is referred to the web version of this article.)

3.4.3. Deep trough and orographic precipitation (4–6 January 2014)

On the 4th of January 2014 the progressive deepening of an Atlantic trough towards east pushed the warm sector of the associated large-scale front towards north-western Italy, determining a sustained advection of humid air masses originating from the south-eastern Mediterranean towards the northern Apennines of Liguria, Emilia Romagna and Toscana regions (Fig. 10c). This dynamic and slowly-moving configuration determined the occurrence of persistent orographic rainfalls over the area, producing large accumulations that caused high river discharge in many catchments, local floodings and several landslides (ARPAL, 2014; ARPAE, 2014).

Likewise to the event described in Section 3.4.1, which was similarly associated with large-scale dynamical systems, the aeral distributions of the accumulated precipitation over three days reported in Fig. 16 show similar features among the different datasets. MOLOCH is the only dataset producing rainfall peaks exceeding 200 mm/72 h as observed in GRIPHO (which reflects the highest intensity score detected in Fig. 13c). However, its spatial distribution is less contiguous and more scattered in smaller and isolated peaks compared to the observations. The other datasets show a less fragmented spatial structure of precipitation, and a common trend to underestimate precipitation intensities over the western regions. Also in this case the ensemble aggregation produces the best spatial correlation coefficient (Fig. 12c), even if very close to MERIDA_HRES, as well as the highest area error score (Fig. 13c).

The comparison of skill scores obtained for the three events analyzed (Figs. 12 and 13) reveals a greater variability among reanalyses – and consequently higher uncertainty - in the representation of local-scale convective precipitation systems compared to synopyically-forced and orographically-induced counterparts. This discrepancy is likely imputable to the inherently lower degree of predictability associated with convective precipitation. Nonetheless, the ensemble aggregation tends to outperform the individual contributions, underscoring the efficacy of combining multiple reanalysis datasets to enhance the representation of precipitation even at the event scale.

4. Discussion

The overarching goal of this study is to present a possible way to integrate the diverse initiatives recently undertaken by the Italian meteorological community, which have culminated in the generation of several regional reanalysis products. The focus lies in determining whether the synergistic use of these datasets can enhance the representation of precipitation. To this end, we conducted a comprehensive analysis employing a MME of four high-resolution CP regional reanalyses, and evaluated multiple aspects of precipitation characteristics across Italy during the period 2007–2016. For comparison, GRIPHO, an hourly observational dataset derived from rain gauge measurements, serves as the reference for observed precipitation.

The MME aggregation improves the representation of precipitation compared to individual datasets. The resultant rainfall estimates demonstrate improved consistency with observational data in terms of

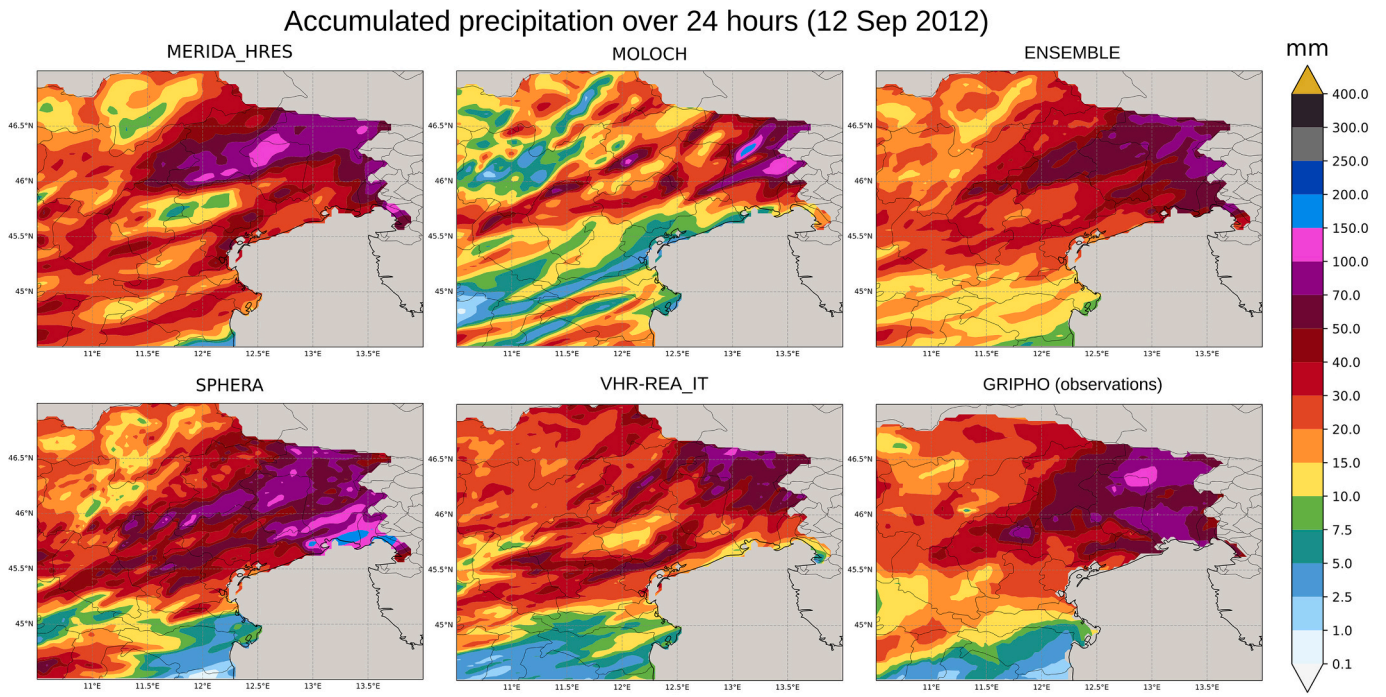

Fig. 15. Same as Fig. 5 but for the accumulated precipitation on the 12th of September 2012 over North-Eastern Italy.

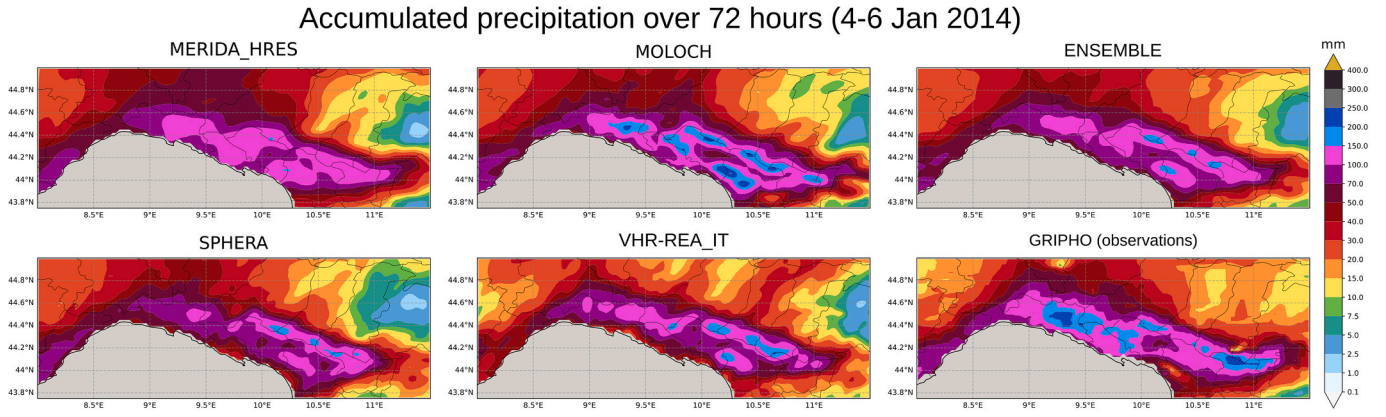

Fig. 16. Same as Fig. 5 but for the accumulated precipitation on 4–6 January 2014 over Liguria and Emilia Romagna regions.

spatial distributions, intensity, and frequency, as evidenced by generally superior skill scores, particularly regarding spatial correlation coefficients, *CRMSE* and ETS metrics. Notably, no single dataset emerges as categorically superior across all precipitation indices, sub-regions of interest, or temporal aggregations. This observation is supported by the findings of Cavalleri et al. (2024b), who present a comparative analysis of the four regional reanalyses included in this study against coarser-resolution datasets. Their research confirms the overall enhancement in daily rainfall representation offered by CP datasets when compared to convection-parameterizing counterparts. However, it also reveals enhanced variability among different reanalysis estimates relative to reference precipitation states at higher resolutions. Similar to our study, this increased degree of dispersion, and consequently lower skill, is most pronounced during the summer season, when the magnitude and localization of deviations from reference states exhibit the highest inter-dataset variability. This is likely attributable to the lower predictability of convective precipitation, which stems from the intrinsic chaotic behavior of the small-scale dynamical processes that govern its formation and development (e.g., Doswell III, 2001). Indeed, summer convective precipitation over Italy is often associated with weak synoptic forcings, allowing the internal dynamics of NWP models to evolve more independently from large-scale inputs. As a result, local-scale processes dominate, and non-linear interactions can amplify small initial differences among numerical solutions, increasing inter-model variability and leading to divergent outcomes (Scinocca et al., 2016; Coppola et al., 2020). In addition to this intrinsic chaotic behavior, structural differences among models (as reported in Table 1) can also contribute significantly to discrepancies between reanalysis products. For instance, Grell et al. (2000) noted that at CP scale, precipitation estimates are unlikely to converge toward a single solution especially

over complex terrains. Similarly, Risanto et al. (2023) showed that varying initial moisture conditions, microphysics, and cumulus schemes in CP NWP simulations of mesoscale convective systems can result in substantial changes in the timing, location and intensity of precipitation. The spatial patterns of inter-reanalysis spread in summer precipitation are particularly pronounced over regions of complex topography, including the Alps, the Apennines, and coastal zones. These areas are characterized by enhanced mesoscale variability, where convective initiation and development are strongly influenced by terrain-induced circulations and land–sea interactions, especially along narrow coastlines (e.g., Rotunno and Ferretti, 2001). Particularly, Barthlott and Kirshbaum (2013) demonstrated that deep convection over Mediterranean islands is highly sensitive to terrain-induced boundary-layer modifications, highlighting the complex interaction between coastal slope and sea-breeze circulations. Therefore, differences among numerical models in how these processes are represented—through varying spatial resolutions, terrain parameterizations, and boundary-layer schemes—can amplify discrepancies in localized precipitation patterns. Furthermore, in lowland areas such as the Po Valley, where strong soil moisture–precipitation coupling during summer has been documented (Seneviratne et al., 2021; Taylor et al., 2012), discrepancies in land-surface models and surface flux formulations may lead to divergent convective responses among the MME members. While the present study does not explicitly isolate these mechanisms, the correspondence between regions of complex terrain and enhanced model spread suggests that such physical processes are contributing factors to the observed inter-model variability.

The added value of the MME is particularly evident right in the warm season, when the error compensation achieved through ensemble combination is more effective, resulting in overall bias reduction. This enhanced performance is likely attributable to the amplified diversity in intensity deviations observed among the estimates of individual ensemble members. This conclusion is reinforced by the comparative analysis of the three case studies detailed in Section 3.4. Specifically, the superior skill of the MME compared to most individual reanalyses is more pronounced for the event characterized by multiple convective storms in late summer. In contrast, events dominated by frontal and orographic precipitation—typical of the fall and winter seasons—show minimal variability among the individual products.

The comparison between the two datasets driven by the same NWP model COSMO (i.e., SPHERA and VHR-REA_IT), and sharing a similar setup (see Table 1), indicates that the inclusion of local-scale data assimilation through nudging does not consistently improve precipitation estimates across all regions. Indeed, a key distinction between these datasets lies in the implementation of a continuous nudging scheme for assimilating observational data at the grid resolution implemented in SPHERA (Giordani et al., 2023), which VHR-REA_IT does not incorporate (Adinolfi et al., 2023). This variation is believed to account for the significant differences detected in the precipitation outputs of the two datasets, highlighting the non-linear effects—both positive and negative—of local data assimilation on simulated precipitation fields. Specifically, SPHERA demonstrates a reduced precipitation bias over the Alpine region and the Mediterranean coasts of Italy, yet it exhibits a pronounced wet bias in the Po Valley. In contrast, VHR-REA_IT mitigates the wet bias over the northern plains while showing increased overestimations over Alpine regions and underestimations over western coastlines. This divergent behavior in precipitation over northern Italy could be attributed to the assimilation of low-level relative humidity observations in SPHERA, alongside the lack of assimilation for two-meter temperature data. Previous research has shown that CP datasets often manifest warm temperature biases in flat terrains, largely due to inaccuracies in the soil moisture-precipitation feedback mechanism when explicitly resolving DMC (Hohenegger et al., 2009; Taylor et al., 2013; Sangelantoni et al., 2023; Adinolfi et al., 2023). In COSMO-based datasets, such as VHR-REA_IT, it has been reported that summer temperature biases in the Po Valley may exceed +2.5 °C (Cavalleri et al., 2024a). Therefore, by correcting the modeled surface humidity while leaving the temperature field unaltered (and, hence, positively biased relative to observations), SPHERA may generate excessive convective precipitation over the northern Italian plains. This could contribute substantially to the detected wet bias, which peaks especially in summer. However, quantitatively assessing this hypothesis poses significant challenges, as it necessitates a sensitivity analysis of the reanalysis production configurations, which would incur prohibitive computational and time costs for the purpose of this study.

In this study the extreme precipitation characteristics are analyzed through the 99th and 99.9th percentile of daily and hourly precipitation distributions, respectively. Our findings reveal that the MME aggregation exhibits a tendency to overly smooth precipitation intensities in comparison to individual datasets, producing contrasting effects across different timescales. For daily precipitation extremes, characterized by a higher degree of statistical dispersion due to the broader ranges that daily-accumulated peaks can reach to, the aggregation process leads to the attenuation of the most extreme peaks identified by individual datasets. This leads to a general shift of the precipitation distribution towards less extreme and more homogeneous values. Conversely, when considering hourly precipitation extremes, we observe an opposite smoothing effect; single-dataset distributions demonstrate less dispersion at hourly temporal frequency, which in turn prompts the MME composite to shift towards uniformly higher extreme distributions relative to individual reanalyses. These findings underscore the necessity of exploring more nuanced methodologies for aggregating precipitation fields, particularly when focusing on extreme precipitation events. The simple concatenation of individual rainfall distributions applied in this analysis may not adequately capture the variability and intensity of extreme precipitation phenomena. Possible future work could aim to develop more sophisticated aggregation techniques that better preserve the characteristics of extreme values in precipitation data in a multi-model framework.

Finally, it is important to acknowledge that the reference observational dataset considered (GRIPHO) is not without its shortcomings. Its inherent deficiencies may contribute to the discrepancies observed in the evaluation of reanalysis datasets. For instance, it has been estimated that the reliability of precipitation data obtained through CP models may substantially outperform that of the observations, particularly in areas characterized by complex topography (Lundquist et al., 2020). Several factors can introduce uncertainties in observational precipitation estimates, especially regarding the underestimation of extreme accumulation events associated with orographic precipitation or localized convective showers (La Barbera et al., 2002; Frei et al., 2003; Prein and Gobiet, 2017). Key contributors to these uncertainties include: heterogeneous spatio-temporal distributions of rain gauges included in the production of the dataset (as in southern Italy, where gauge density is lower compared to northern regions, or in mountainous regions compared to plains, and where the number of gauges increased from approximately 500 in 2001 to about 2600 in 2012 – Fantini, 2019); undercatch phenomena due to wind-induced effects on raindrop collection; instrumental errors; potential losses from sensor wetting or droplets evaporation; and the inherent smoothing of the precipitation field resulting from the interpolation process that seeks to uniform the sparse gauge network into a consistent regular grid. These factors highlight the complexities involved in accurately capturing precipitation and reinforce the need for caution when interpreting the results of reanalysis rainfall estimates in relation to observational references.

5. Conclusion

The analysis of a MME of high-resolution regional reanalysis datasets over Italy presented in this work demonstrates the added value in describing more effectively rainfall patterns through a multi-dataset aggregation. Indeed, when compared to the reference observational analysis GRIPHO over a decade-long period, the ensemble demonstrates

higher performance relative to individual CP datasets. This is evident in the enhanced representation of spatial precipitation distributions, both for daily and hourly estimates, in terms of their intensity and frequency of occurrence, for the reproduction of daily cycles of summer precipitation, as well as for the effective representation of recent significant high-impact precipitation events. The error compensation operated by the MME aggregation is attributable to the substantial variability in the representation of rainfall among individual reanalysis datasets, particularly during summer, associated with the more chaotic dynamics characterizing convective precipitation.

A potential caveat of this approach could be given by the mixing of multiple physical systems through the MME, which, besides compensating the error in rainfall estimates, could introduce artificial deviations from a physically consistent representation. For this reason, the method should be tested with a broader case-study analysis to investigate the systematic trend of the MME approach more robustly. Additionally, the promising findings of this study could be further substantiated by increasing the number of datasets incorporated into the ensemble. A broader selection of datasets would not only enhance the sampling of internal variability inherent to multiple numerical simulations, but also augment the diversity of physical atmospheric representations achieved through various NWP models. In this analysis, we considered four datasets, a number that may limit our ability to comprehensively describe precipitation variability in the atmosphere, particularly during the convective season. The warm season is indeed characterized by pronounced uncertainty in precipitation representation, largely due to the inherent limits in predictability of chaotic convective processes, resulting in significant variability among datasets. Potential datasets that could futher enrich this analysis include MORE, a high-resolution retrospective dataset based on the MOLOCH model and currently in production at the ISAC-CNR institute (Stocchi and Davolio, 2023). Another valuable resource is the newly released Computational Hydrometeorology with Advanced Performance to Enhanced Realism (CHAPTER) dataset, consisting of a dynamical downscaling of ERA5 using WRF over Europe and the Mediterranean area, produced at the Liebniz Supercomputing Center (Bernini et al., 2025). Additionally, the production of a new CP reanalysis over Italy considering the limited-area model ICOsahedral Non-hydrostatic model (ICON) has recently been planned by the ItaliaMeteo national agency for meteorology and climate (Giordani et al., 2025). This initative aligns with efforts at the Deutscher WetterDienst (DWD), specifically the development of the Fine-scale Observation-based Reanalysis for Central Europe (ICON-FORCE), a new regional reanalysis centered over Germany (Valmassoi et al., 2025). In this context, the effectiveness of the MME approach could be further assessed by applying it in different regions of the world where comparable high-resolution datasets are available. For instance, a MME constructed over Germany considering e.g. ICON-FORCE, COSMO-REA2 (Wahl et al., 2017), and CHAPTER could provide valuable insights. Similarly, a corresponding analysis over the United States—incorporating regional products such as HRRR (Dowell et al., 2022), ADDA_V2 (Akinsanola et al., 2024) or CONUS404 (Rasmussen et al., 2023)—could demonstrate the broader applicability and robustness of the MME methodology across different climatic and geographic settings.

Improving the description of past meteorological conditions using reanalysis datasets is essential for accurate atmospheric characterization. In particular, their combined application—as demonstrated in this study—enhances the reliability of estimates and associated uncertainties. This approach supports climate pattern monitoring across multiple spatial scales, from planetary to local, and provides potential datasets for training and developing next-generation artificial-intelligence-based data-driven models (e.g. Lang et al., 2024). The MME methodology also aids in exploring potential future scenarios that account for the impacts of climate change on system evolution, particularly by evaluating deviations from forward NWP model outputs with historical baselines. The advantages of this comprehensive perspective extend beyond meteorological and climate-related applications; they also offer considerable value for downstream modeling efforts that rely on meteorological inputs. In this context, individual Italian reanalysis datasets have recently been employed in various fields, that led to promising results, such as: the study of hail-favouring convective environments for estimating the probability of hailstorms (Giordani et al., 2024), the production of wind atlases to support the design of wind energy parks (Pavan et al., 2024; Sperati et al., 2024), the monitoring of water resources (Citrini et al., 2024), and the assessment of hydrogeological risk (Abbate et al., 2024). Employing multiple products concurrently could therefore further improve the estimates obtained for similar applications. For instance, in flood forecasting, meteorological models are typically integrated with hydrological and hydraulic models to assess precipitation dynamics within a watershed and predict subsequent impacts on specific regions (e.g. Lobligeois et al., 2014). Forcing a flood forecasting systems with meteorological MMEs have already demonstrated improvements in reliably assessing discharge peaks predictions for warning purposes (Diomede et al., 2008; Zsótér et al., 2016). Furthermore, recent research have underscored the value of employing global and regional meteorological reanalyses for hydrological modeling, particularly in regions with limited observational data (Essou et al., 2016; Andreadis et al., 2017; Nkiaka et al., 2017; Tarek et al., 2020). Hence, by incorporating multiple precipitation estimates derived from a meteorological MME of high-resolution reanalysis datasets, we could improve the assessment of impacts and associated uncertainties related to past extreme precipitation events over hydrological catchments. This integration may not only enhance the representation of historical flood events but also improve our understanding to produce better flood forecasts in the present.

Funding information

This study was supported by the European Union NextGenerationEU/NRRP, Mission 4 Component 2 Investment 1.5, Call 3277 (12/30/2021), Award 0001052 (06/23/2022), under the project ECS00000033 “Ecosystem for Sustainable Transition in Emilia-Romagna” (ECOSISTER), Spoke 6 “Ecological Transition Based on HPC and Data Technology”, and by the Alma Mater Studiorum – University of Bologna, under the project SINTESI, with a grant Alma CaReS (Cambiamenti climatici, Resilienza, Sostenibilità) 2023.

CRediT authorship contribution statement

Antonio Giordani: Writing – review & editing, Writing – original draft, Visualization, Validation, Software, Methodology, Investigation, Formal analysis, Data curation, Conceptualization. **Paolo Ruggieri:** Funding acquisition, Supervision, Project administration, Conceptualization. **Silvana Di Sabatino:** Conceptualization, Supervision, Project administration, Funding acquisition.

Declaration of competing interest

The authors declare that they have no known competing financial interests or personal relationships that could have appeared to influence the work reported in this paper.

Appendix A

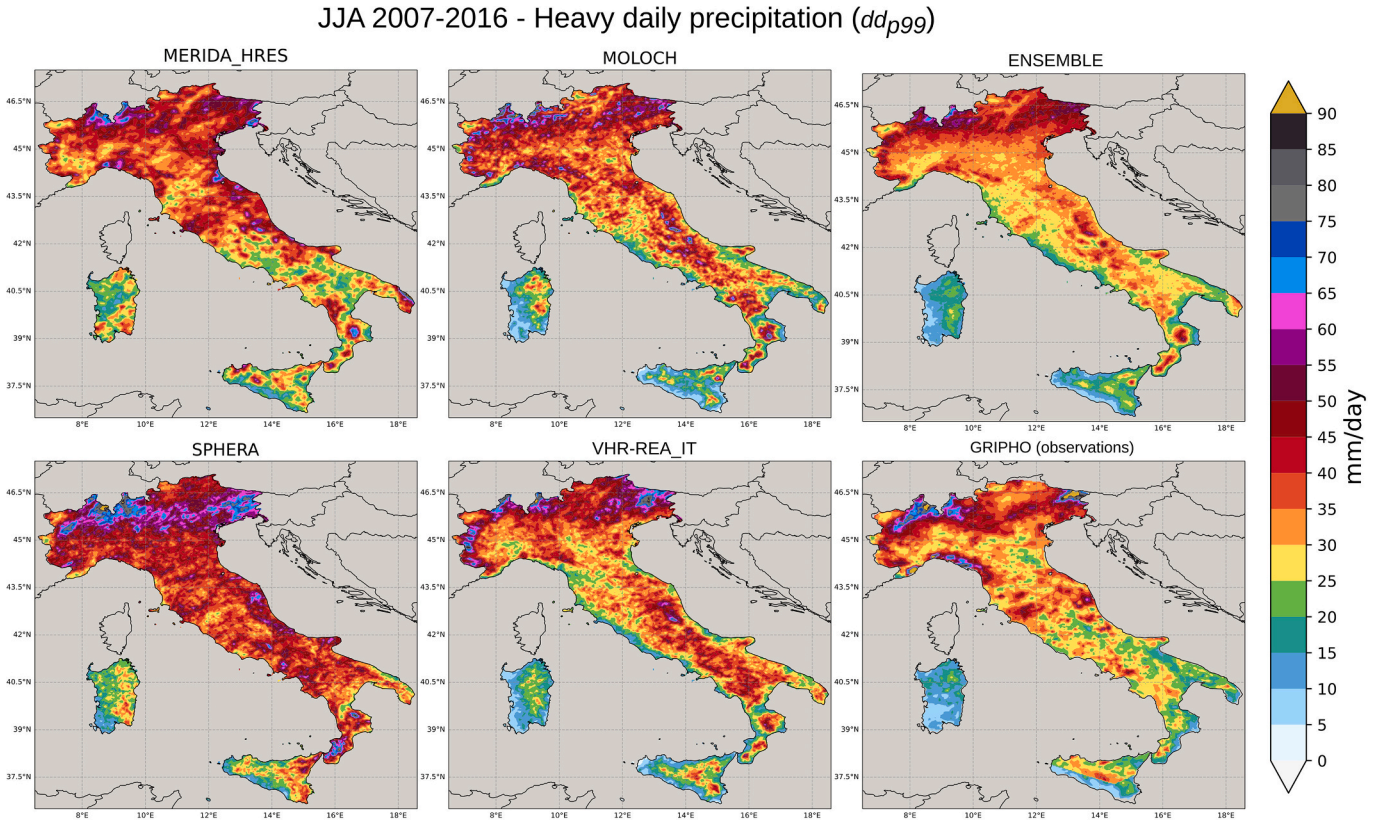

Fig. A1. Same as Fig. 5 but for heavy daily precipitation (dd_{p99}) in JJA.

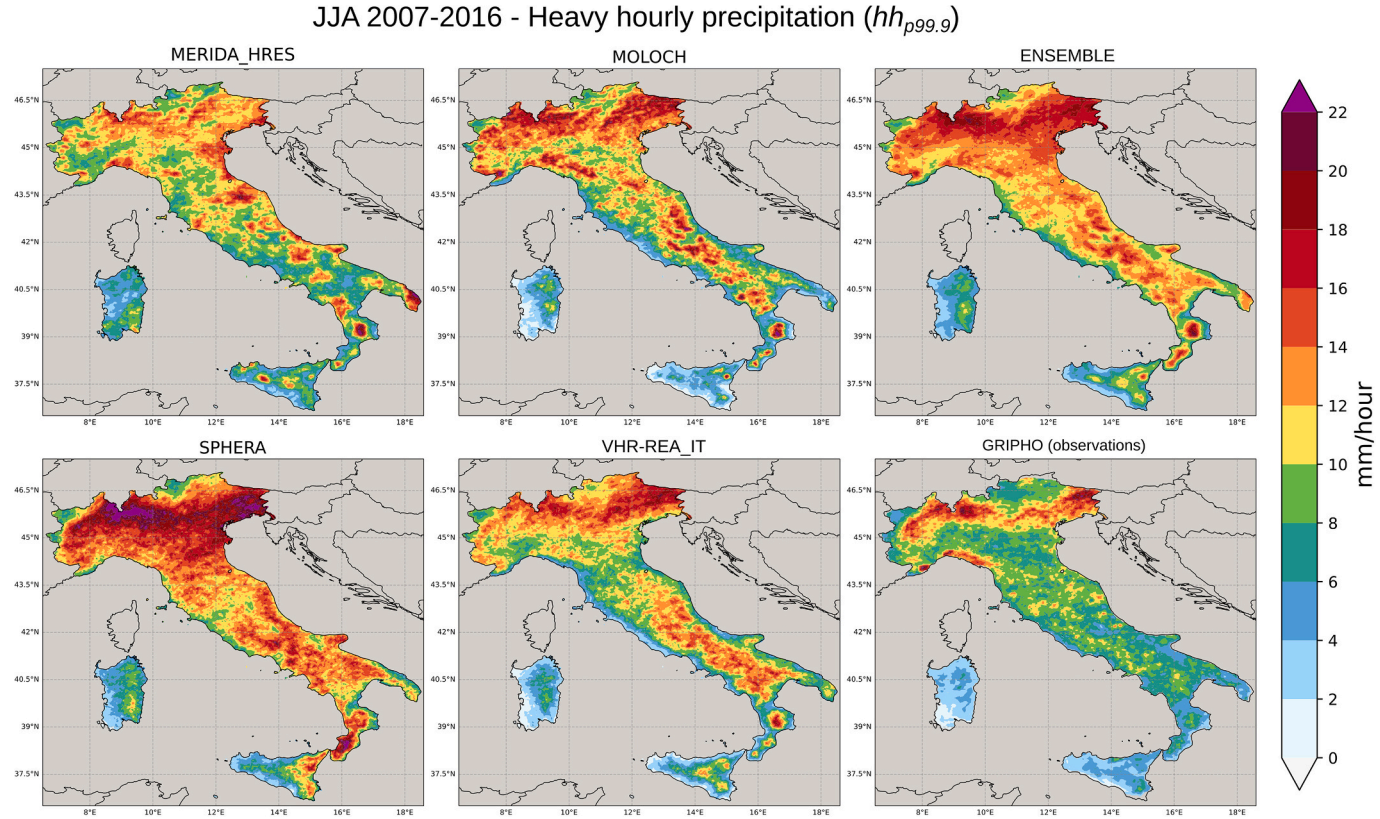

Fig. A2. Same as Fig. 5 but for heavy hourly precipitation ($hh_{p99.9}$) in JJA.

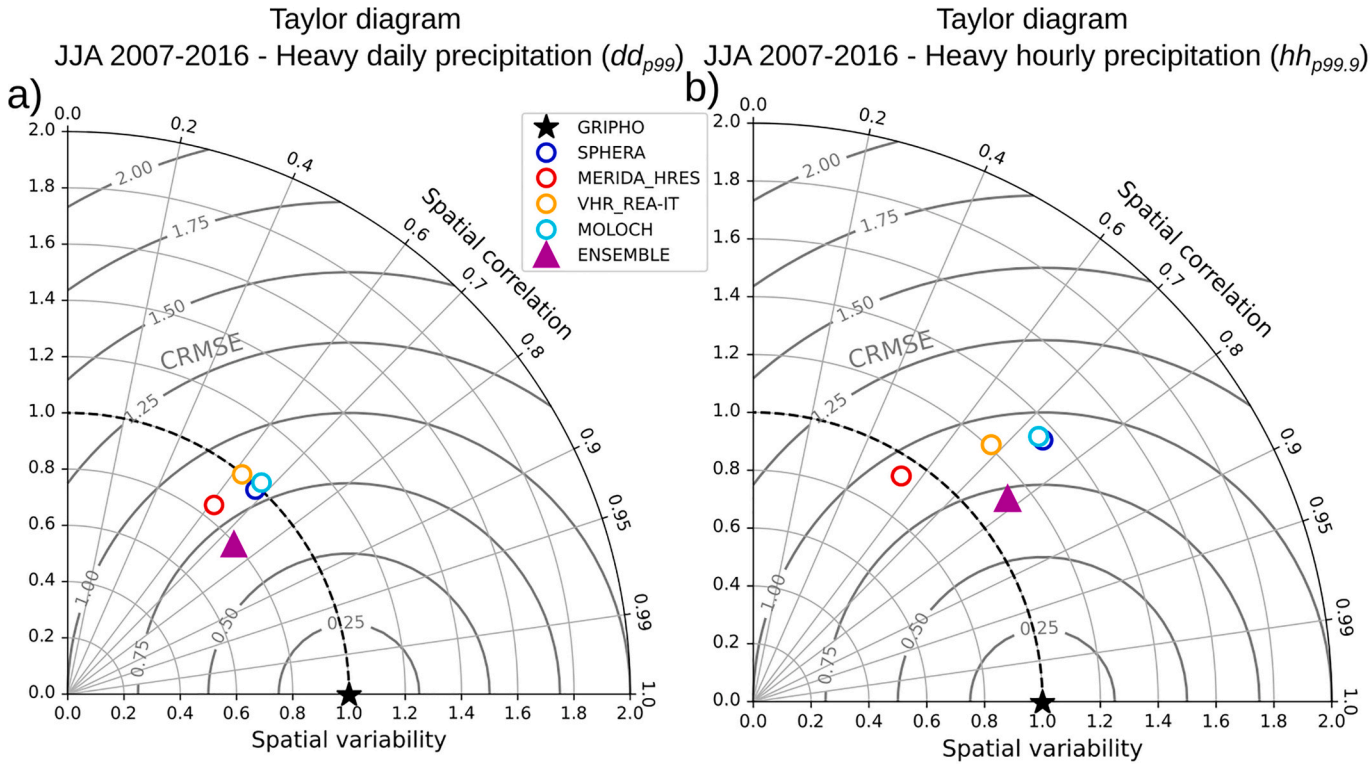

Fig. A3. Same as Fig. 6 but: a) for the JJA spatial distributions of dd_{p99} (Fig. A1), b) for the JJA spatial distributions of $hh_{p99.9}$ (Fig. A2).

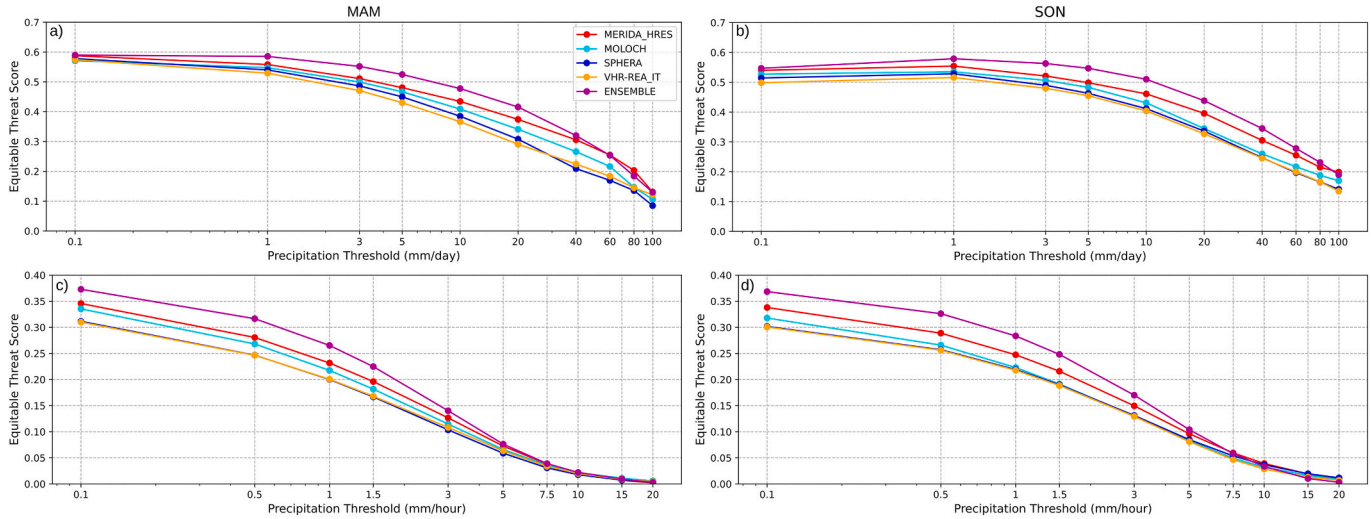

Fig. A4. Same as Fig. 4 but for MAM (a-c) and SON (b-d).

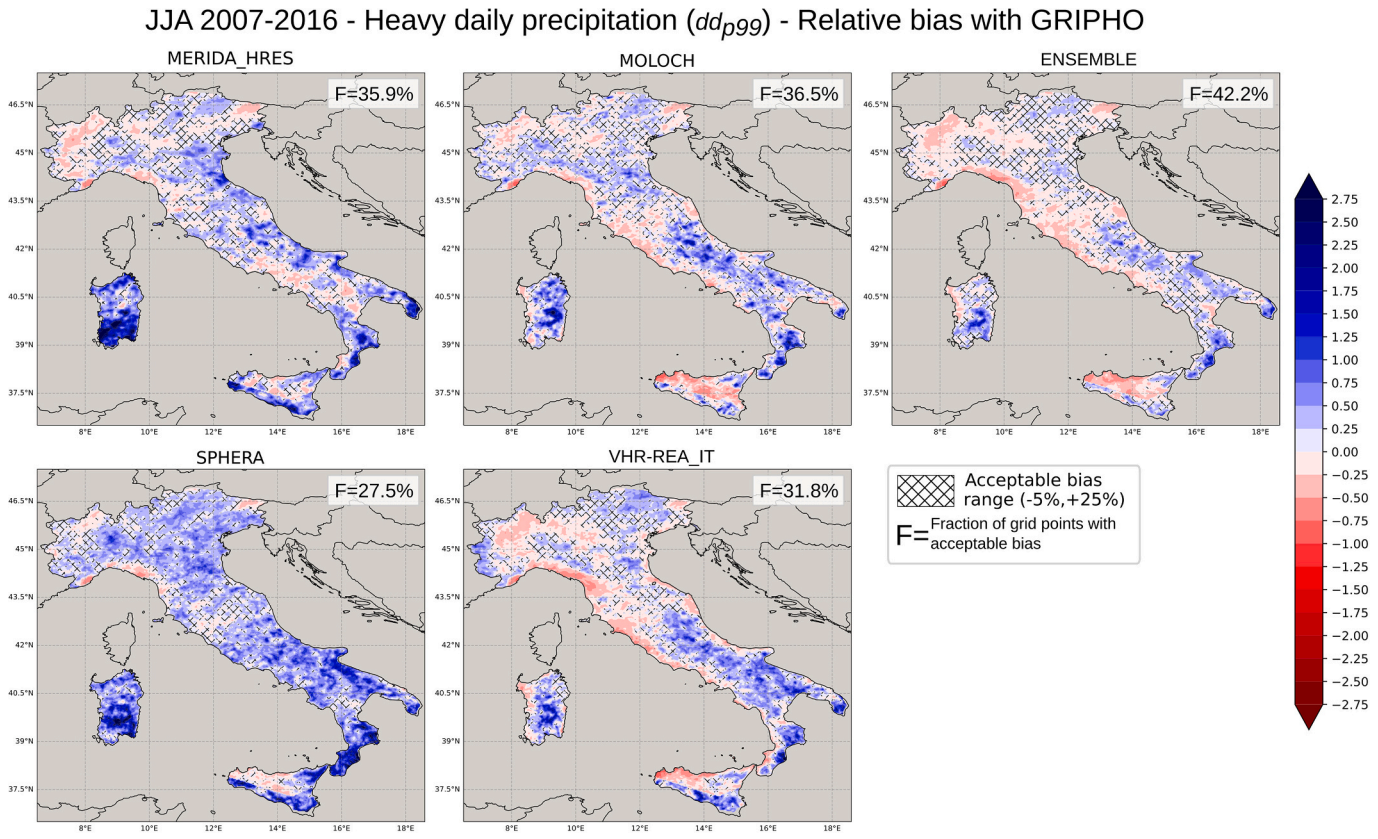

Fig. A5. Same as Fig. 7 but for heavy daily precipitation (dd_{p99}) in JJA.

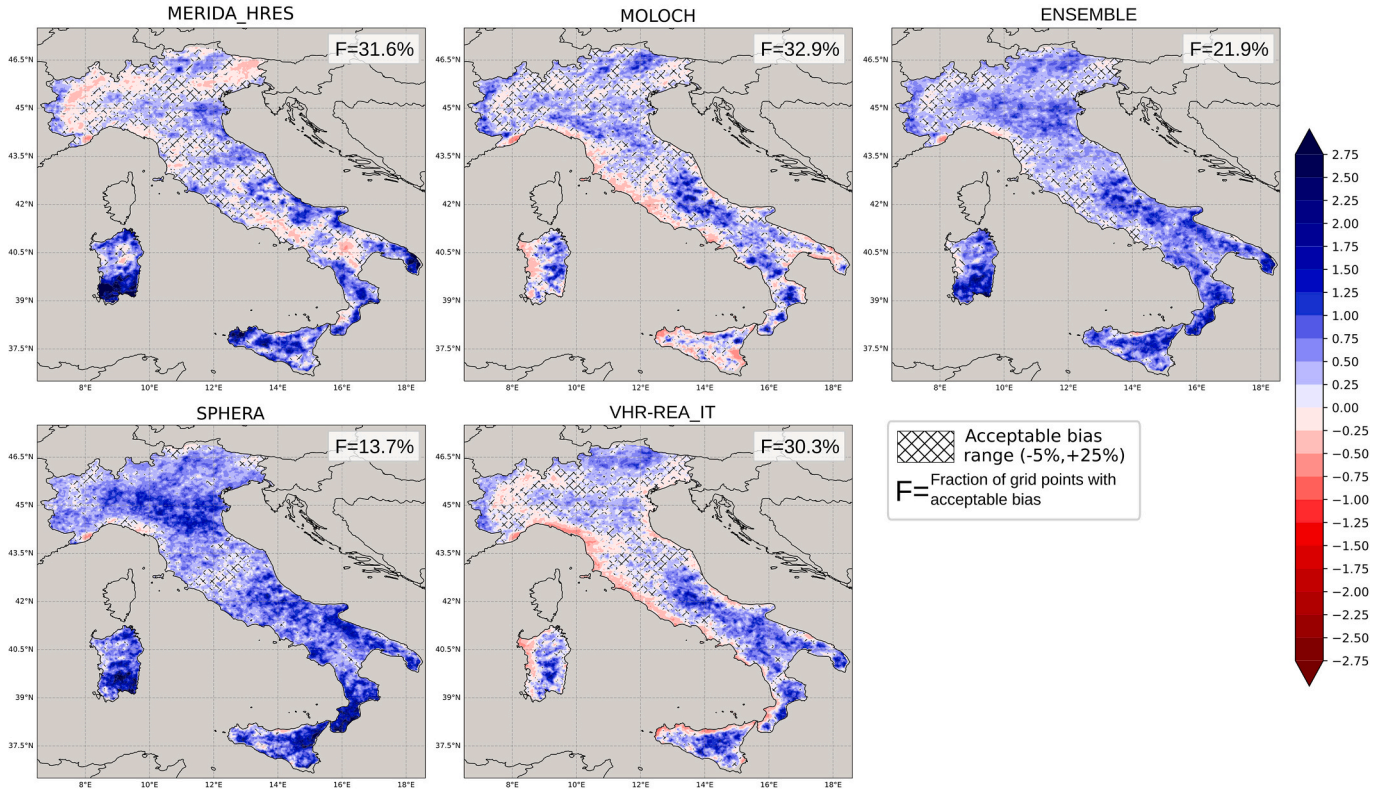

Fig. A6. Same as Fig. 7 but for heavy hourly precipitation (hh_{p99}) in JJA.

Data availability

The hourly precipitation data from the MME mean of the four datasets is openly available via the Zenodo repository at: https://doi.org/10.5281/zenodo.15745597

GRIPHO observational data have been made available upon request by the ICTP institute.

MERIDA_HRES data is openly available via the RSE repository at: https://merida.rse-web.it/

MOLOCH data is openly available via the Zenodo repository at: https://doi.org/10.5281/zenodo.14250195

SPHERA data is openly available via the Zenodo repository at: https://doi.org/10.5281/zenodo.10441408.

VHR-REA_IT data is openly available via CMCC Data Delivery System at: https://dds.cmcc.it/#/dataset/era5-downscaled-over-italy.

References

Abbate, A., Mancusi, L., Frigerio, A., Papini, M., Longoni, L., 2024. CRHyME (Climatic Rainfall Hydrogeological Model Experiment): a new model for geo-hydrological hazard assessment at the basin scale. Nat. Hazards Earth Syst. Sci. Discus. 2023, 1–51.

Adinolfi, M., Raffa, M., Reder, A., Mercogliano, P., 2023. Investigation on potential and limitations of ERA5 Reanalysis downscaled on Italy by a convection-permitting model. Clim. Dyn. 61 (9), 4319–4342.

Akinsanola, A.A., Jung, C., Wang, J., Kotamarthi, V.R., 2024. Evaluation of precipitation across the contiguous United States, Alaska, and Puerto Rico in multi-decadal convection-permitting simulations. Sci. Rep. 14 (1), 1238.

Andreadis, K.M., Schumann, G.J.P., Stampoulis, D., Bates, P.D., Brakenridge, G.R., Kettner, A.J., 2017. Can atmospheric reanalysis data sets be used to reproduce flooding over large scales? Geophys. Res. Lett. 44 (20), 10–369.

ARPAE, 2013. Regional agency for environmental protection of Emilia Romagna. In: Rapporto dell'evento idrologico e meteo-marino del 10–12 novembre 2013. Technical Report. https://www.arpae.it/it/temi-ambientali/meteo/report-meteo/rapporti-post-evento/rapporto-2013-26-dellevento-dal-10-al-12-novembre-2013/view [Accessed 2nd July 2025].

ARPAE, 2014. Regional agency for environmental protection of Emilia Romagna. In: Rapporto sull'evento meteorologico, idrogeologico e idraulico del 4–6 gennaio 2014. Technical Report. https://www.arpae.it/it/temi-ambientali/meteo/report-meteo/rapporti-post-evento/rapporto-2014-01-dellevento-dal-04-al-06-gennaio-2014/view [Accessed 2nd July 2025].

ARPAL, 2014. Regiona agency for environmental protection of Liguria. In: Rapporto di evento meteoidrologico del 04–05/01/2014. Technical Report. https://www.arpal.liguria.it/contenuti_statici//pubblicazioni/rapporti_eventi/2014/REM_20140104-05_allerta1ABD-allerta2CE_vers20140217.pdf [Accessed 2nd July 2025].

Ban, N., Schmidli, J., Schär, C., 2014. Evaluation of the convection-resolving regional climate modeling approach in decade-long simulations. J. Geophys. Res. Atmos. 119 (13), 7889–7907.

Ban, N., Caillaud, C., Coppola, E., Pichelli, E., Sobolowski, S., Adinolfi, M., Zander, M.J., 2021. The first multi-model ensemble of regional climate simulations at kilometer-scale resolution, part I: evaluation of precipitation. Clim. Dyn. 57, 275–302.

Barthlott, C., Kirshbaum, D.J., 2013. Sensitivity of deep convection to terrain forcing over Mediterranean islands. Q. J. R. Meteorol. Soc. 139 (676), 1762–1779.

Berg, P., Wagner, S., Kunstmann, H., Schädler, G., 2013. High resolution regional climate model simulations for Germany: Part I—validation. Clim. Dyn. 40, 401–414.

Bernini, L., Lagasio, M., Milelli, M., Oberto, E., Parodi, A., Hachinger, S., Tartaglione, N., 2025. Convection-permitting dynamical downscaling of ERA5 for Europe and the Mediterranean basin. Q. J. R. Meteorol. Soc. e5014.

Bonanno, R., Lacavalla, M., Sperati, S., 2019. A new high-resolution meteorological reanalysis Italian Dataset: MERIDA. Q. J. R. Meteorol. Soc. 145 (721), 1756–1779.

Brisson, E., Van Weverberg, K., Demuzere, M., Devis, A., Saeed, S., Stengel, M., van Lipzig, N.P., 2016. How well can a convection-permitting climate model reproduce decadal statistics of precipitation, temperature and cloud characteristics? Clim. Dyn. 47, 3043–3061.

Buzzi, A., Davolio, S., Malguzzi, P., Drofa, O., Mastrangelo, D., 2014. Heavy rainfall episodes over Liguria in autumn 2011: numerical forecasting experiments. Nat. Hazards Earth Syst. 14 (5), 1325–1340.

Caillaud, C., Somot, S., Douville, H., Alias, A., Bastin, S., Brienen, S., de Vries, H., 2024. Northwestern Mediterranean heavy precipitation events in a warmer climate: robust versus uncertain changes with a large convection-permitting model ensemble. Geophys. Res. Lett. 51 (6), e2023GL105143.

Capecchi, V., 2021. Reforecasting two heavy-precipitation events with three convection-permitting ensembles. Weather Forecast. 36 (3), 769–790.

Capecchi, V., Pasi, F., Gozzini, B., Brandini, C., 2023. A convection-permitting and limited-area model hindcast driven by ERA5 data: precipitation performances in Italy. Clim. Dyn. 61 (3), 1411–1437.

Cavalleri, F., Viterbo, F., Brunetti, M., Bonanno, R., Manara, V., Lussana, C., Lacavalla, M., Maugeri, M., 2024a. Inter-comparison and validation of high-resolution surface air temperature reanalysis fields over Italy. Int. J. Climatol. 44 (8), 2681–2700. https://doi.org/10.1002/joc.8475.

Cavalleri, F., Lussana, C., Viterbo, F., Brunetti, M., Bonanno, R., Manara, V., Maugeri, M., 2024b. Multi-scale assessment of high-resolution reanalysis precipitation fields over Italy. Atmos. Res. 312, 107734.

Cerenzia, I.M.L., Pincini, G., Paccagnella, T., Minguzzi, E., Gastaldo, T., Poli, V., Cesari, D., 2020. Forecast of precipitation for the 1994 flood in Piedmont: performance of an ensemble system at convection-permitting resolution. Bull. Atmos. Sci. Technol. 1 (3), 319–338.

Cerenzia, I.M.L., Giordani, A., Paccagnella, T., Montani, A., 2022. Towards a convection permitting regional reanalysis over the Italian domain. In: Manuscript Submitted for Publication to Meteorological Applications.

Chernokulsky, A., Kozlov, F., Zolina, O., Bulygina, O., Mokhov, I.I., Semenov, V.A., 2019. Observed changes in convective and stratiform precipitation in Northern Eurasia over the last five decades. Environ. Res. Lett. 14 (4), 045001.

Citrini, A., Camera, C.A.S., Beretta, G.P., Spalla, M.I., 2024. Modelling current and future water resources availability in an Alpine catchment exploited for hydropower production. PhD thesis. Università degli Studi di Milano. Dipartimento di Scienze della Terra Ardito Desio, 36. ciclo. https://hdl.handle.net/2434/1049328 [Accessed 2nd July 2025].

Clark, P., Roberts, N., Lean, H., Ballard, S.P., Charlton-Perez, C., 2016. Convection-permitting models: a step-change in rainfall forecasting. Meteorol. Appl. 23 (2), 165–181.

Collier, E., Ban, N., Richter, N., Ahrens, B., Chen, D., Chen, X., Ziska, C., 2024. The first ensemble of kilometer-scale simulations of a hydrological year over the third pole. Clim. Dyn. 1–18.

Coppola, E., Sobolowski, S., Pichelli, E., Raffaele, F., Ahrens, B., Anders, I., Warrach-Sagi, K., 2020. A first-of-its-kind multi-model convection permitting ensemble for investigating convective phenomena over Europe and the Mediterranean. Clim. Dyn. 55, 3–34.

Cremonini, L., Randi, P., Fazzini, M., Nardino, M., Rossi, F., Georgiadis, T., 2024. Causes and impacts of flood events in Emilia-Romagna (Italy) in May 2023. Land 13 (11), 1800.

Crespi, A., Brunetti, M., Lentini, G., Maugeri, M., 2018. 1961–1990 high-resolution monthly precipitation climatologies for Italy. Int. J. Climatol. 38 (2), 878–895.

Davolio, S., Malguzzi, P., Drofa, O., Mastrangelo, D., Buzzi, A., 2020. The Piedmont flood of November 1994: A testbed of forecasting capabilities of the CNR-ISAC meteorological model suite. Bull. Atmos. Sci. Technol. 1, 263–282.

Dee, D.P., Uppala, S.M., Simmons, A.J., Berrisford, P., Poli, P., Kobayashi, S., Vitart, F., 2011. The ERA-Interim reanalysis: Configuration and performance of the data assimilation system. Q. J. R. Meteorol. Soc. 137 (656), 553–597.

Deser, C., Phillips, A., Bourdette, V., Teng, H., 2012. Uncertainty in climate change projections: the role of internal variability. Clim. Dyn. 38, 527–546.

Deser, C., Phillips, A.S., Alexander, M.A., Smoliak, B.V., 2014. Projecting North American climate over the next 50 years: uncertainty due to internal variability. J. Clim. 27 (6), 2271–2296.

Diaconescu, E.P., Gachon, P., Laprise, R., 2015. On the remapping procedure of daily precipitation statistics and indices used in regional climate model evaluation. J. Hydrometeorol. 16 (6), 2301–2310.

Diomede, T., Davolio, S., Marsigli, C., Miglietta, M.M., Moscatello, A., Papetti, P., Malguzzi, P., 2008. Discharge prediction based on multi-model precipitation forecasts. Meteorog. Atmos. Phys. 101, 245–265.

Doms, G., Förstner, J., Heise, E., Herzog, H.J., Mironov, D., Raschendorfer, M., Vogel, G., 2011. A description of the nonhydrostatic regional COSMO model. In: Part II: Physical Parameterization. Deutscher Wetterdienst, Offenbach, Germany.

Doswell III, C.A., 2001. Severe convective storms—an overview. In: Severe Convective Storms. Springer, pp. 1–26.

Dowell, D.C., Alexander, C.R., James, E.P., Weygandt, S.S., Benjamin, S.G., Manikin, G. S., Alcott, T.I., 2022. The High-Resolution Rapid Refresh (HRRR): an hourly updating convection-allowing forecast model. Part I: Motivation and system description. Weather Forecast. 37 (8), 1371–1395.

Drofa, O.V., Malguzzi, P., 2004. Parameterization of microphysical processes in a non hydrostatic prediction model. In: Proceedings of 14th Intern. Conf. on Clouds and Precipitation (ICCP), Bologna, Italy, pp. 19–23.

Ducrocq, V., Nuissier, O., Ricard, D., Lebeaupin, C., Thouvenin, T., 2008. A numerical study of three catastrophic precipitating events over southern France. II: Mesoscale triggering and stationarity factors. Quart. J. Royal Meteorol. Soc. J. Atmosph. Sci. Appl. Meteorol. Phys. Oceanogr. 134 (630), 131–145.

Ebert, E.E., McBride, J.L., 2000. Verification of precipitation in weather systems: determination of systematic errors. J. Hydrol. 239 (1–4), 179–202.

Essou, G.R., Sabarly, F., Lucas-Picher, P., Brissette, F., Poulin, A., 2016. Can precipitation and temperature from meteorological reanalyses be used for hydrological modeling? J. Hydrometeorol. 17 (7), 1929–1950.

Fantini, A., 2019. Climate change impact on flood hazard over Italy. Ph.D. thesis. In: Università degli studi di Trieste. http://hdl.handle.net/11368/2940009 [Accessed 2nd July 2025].

Ferrett, S., Frame, T.H., Methven, J., Holloway, C.E., Webster, S., Stein, T.H., Cafaro, C., 2021. Evaluating convection-permitting ensemble forecasts of precipitation over Southeast Asia. Weather Forecast. 36 (4), 1199–1217.

Ferretti, R., Pichelli, E., Gentile, S., Maiello, I., Cimini, D., Davolio, S., Rotunno, R., 2014. Overview of the first HyMeX Special Observation Period over Italy: observations and model results. Hydrol. Earth Syst. Sci. 18 (5), 1953–1977.

Fosser, G.S.K.P.B., Khodayar, S., Berg, P., 2015. Benefit of convection permitting climate model simulations in the representation of convective precipitation. Clim. Dyn. 44, 45–60.

Fowler, H.J., Ekström, M., Blenkinsop, S., Smith, A.P., 2007. Estimating change in extreme European precipitation using a multimodel ensemble. J. Geophys. Res. Atmos. 112 (D18).

Frei, C., Christensen, J.H., Déqué, M., Jacob, D., Jones, R.G., Vidale, P.L., 2003. Daily precipitation statistics in regional climate models: Evaluation and intercomparison for the European Alps. J. Geophys. Res. Atmos. 108 (D3).
Gimeno, L., Sorí, R., Vazquez, M., Stojanovic, M., Algarra, I., Eiras-Barca, J., Nieto, R., 2022. Extreme precipitation events. Wiley Interdiscip. Rev. Water 9 (6), e1611.
Giordani, A., Cerenzia, I.M.L., Paccagnella, T., Di Sabatino, S., 2023. SPHERA, a new convection-permitting regional reanalysis over Italy: Improving the description of heavy rainfall. Q. J. R. Meteorol. Soc. 149 (752), 781–808.
Giordani, A., Kunz, M., Bedka, K.M., Punge, H.J., Paccagnella, T., Pavan, V., Di Sabatino, S., 2024. Characterizing hail-prone environments using convection-permitting reanalysis and overshooting top detections over south-central Europe. Nat. Hazards Earth Syst. Sci. 24 (7), 2331–2357.
Giordani, A., Capecchi, V., Gastaldo, T., Poli, V., Vittorioso, F., 2025. I-DREAM-IT: a new convection-permitting limited-area atmospheric reanalysis over Italy using ICON-DREAM reanalysis as boundary conditions and the ICON-2I meteorological model. Request for a special project. ECMWF. https://www.ecmwf.int/sites/default/files/special_projects/2026/spitgior-2026-request.pdf (Accessed 2nd July 2025).
Giovannini, L., Davolio, S., Zaramella, M., Zardi, D., Borga, M., 2021. Multi-model convection-resolving simulations of the October 2018 Vaia storm over Northeastern Italy. Atmos. Res. 253, 105455.
Gleeson, E., Whelan, E., Hanley, J., 2017. Met Éireann high resolution reanalysis for Ireland. Adv. Sci. Res. 14, 49–61.
Grazzini, F., Craig, G.C., Keil, C., Antolini, G., Pavan, V., 2020a. Extreme precipitation events over northern Italy. Part I: A systematic classification with machine-learning techniques. Q. J. R. Meteorol. Soc. 146 (726), 69–85.
Grazzini, F., Fragkoulidis, G., Pavan, V., Antolini, G., 2020b. The 1994 Piedmont flood: an archetype of extreme precipitation events in Northern Italy. Bull. Atmos. Sci. Technol. 1, 283–295.
Grell, G.A., Schade, L., Knoche, R., Pfeiffer, A., Egger, J., 2000. Nonhydrostatic climate simulations of precipitation over complex terrain. J. Geophys. Res. Atmos. 105 (D24), 29595–29608.
Greybush, S.J., Saslo, S., Grumm, R., 2017. Assessing the ensemble predictability of precipitation forecasts for the January 2015 and 2016 East Coast winter storms. Weather Forecast. 32 (3), 1057–1078.
Han, X., Xue, H., Zhao, C., Lu, D., 2016. The roles of convective and stratiform precipitation in the observed precipitation trends in Northwest China during 1961–2000. Atmos. Res. 169, 139–146.
Hawkins, E., Sutton, R., 2009. The potential to narrow uncertainty in regional climate predictions. Bull. Am. Meteorol. Soc. 90 (8), 1095–1108.
Hersbach, H., Bell, B., Berrisford, P., Hirahara, S., Horányi, A., Muñoz-Sabater, J., Simmons, A., 2020. The ERA5 global reanalysis. Q. J. R. Meteorol. Soc. 146 (730), 1999–2049.
Hohenegger, C., Brockhaus, P., Bretherton, C.S., Schär, C., 2009. The soil moisture–precipitation feedback in simulations with explicit and parameterized convection. J. Clim. 22 (19), 5003–5020.
Holloway, C.E., Neelin, J.D., 2009. Moisture vertical structure, column water vapor, and tropical deep convection. J. Atmos. Sci. 66 (6), 1665–1683.
Hong, S.Y., Noh, Y., Dudhia, J., 2006. A new vertical diffusion package with an explicit treatment of entrainment processes. Mon. Weather Rev. 134 (9), 2318–2341.
Iacono, M.J., Delamere, J.S., Mlawer, E.J., Shephard, M.W., Clough, S.A., Collins, W.D., 2008. Radiative forcing by long-lived greenhouse gases: calculations with the AER radiative transfer models. J. Geophys. Res. Atmos. 113 (D13103).
Isotta, F.A., Frei, C., Weilguni, V., Perčec Tadić, M., Lassegues, P., Rudolf, B., Vertačnik, G., 2014. The climate of daily precipitation in the Alps: development and analysis of a high-resolution grid dataset from pan-Alpine rain-gauge data. Int. J. Climatol. 34 (5), 1657–1675.
Kendon, E.J., Fosser, G., Murphy, J., Chan, S., Clark, R., Harris, G., Lock, A., Lowe, J., Martin, G., Pirret, J., Roberts, N., Sanderson, M., Tucker, S., 2019. UKCP Convection-permitting model projections: science report. In: UK Met Office. URL. https://www.metoffice.gov.uk/pub/data/weather/uk/ukcp18/science-reports/UKCP-Convection-permitting-model-projections-report.pdf (Accessed 2nd July 2025).
Kendon, E.J., Short, C., Pope, J., Chan, S.C., Wilkinson, J., Tucker, S., Bett, P., Harris, G., Murphy, J., 2021. Update to ukcp local (2.2km) projections. In: Technical report, United Kingdom Met Office, Exeter, United Kingdom, 7. URL. https://www.metoffice.gov.uk/research/approach/collaboration/ukcp/guidance-science-reports [Accessed 2nd July 2025].
Kerkmann, J., Setvák, M., Manzato, A., 2012. Experimental 2.5-minute super rapid scans from MSG-3 capture a supercell storm above northern Italy (12 September 2012). In: EUMETSAT Report. Available online at https://user.eumetsat.int/resources/case-studies/experimental-2-5-minute-super-rapid-scans [Accessed 2nd July 2025].
Kim, Y.T., Yu, J.U., Kim, T.W., Kwon, H.H., 2024. A novel approach to a multi-model ensemble for climate change models: perspectives on the representation of natural variability and historical and future climate. Weather Clim. Extrem. 44, 100688.
Kirshbaum, D.J., Adler, B., Kalthoff, N., Barthlott, C., Serafin, S., 2018. Moist orographic convection: physical mechanisms and links to surface-exchange processes. Atmosphere 9 (3), 80.
Klasa, C., Arpagaus, M., Walser, A., Wernli, H., 2018. An evaluation of the convection-permitting ensemble COSMO-E for three contrasting precipitation events in Switzerland. Q. J. R. Meteorol. Soc. 144 (712), 744–764.
Kotlarski, S., Keuler, K., Christensen, O.B., Colette, A., Déqué, M., Gobiet, A., Wulfmeyer, V., 2014. Regional climate modeling on European scales: a joint standard evaluation of the EURO-CORDEX RCM ensemble. Geosci. Model Dev. 7 (4), 1297–1333.
La Barbera, P., Lanza, L.G., Stagi, L., 2002. Tipping bucket mechanical errors and their influence on rainfall statistics and extremes. Water Sci. Technol. 45 (2), 1–9.
Lang, S., Alexe, M., Chantry, M., Dramsch, J., Pinault, F., Raoult, B., Rabier, F., 2024. AIFS–ECMWF's data-driven forecasting system. arXiv preprint arXiv:2406.01465.
Leutwyler, D., Lüthi, D., Ban, N., Fuhrer, O., Schär, C., 2017. Evaluation of the convection-resolving climate modeling approach on continental scales. J. Geophys. Res. Atmos. 122 (10), 5237–5258.
Lobligeois, F., Andréassian, V., Perrin, C., Tabary, P., Loumagne, C., 2014. When does higher spatial resolution rainfall information improve streamflow simulation? An evaluation using 3620 flood events. Hydrol. Earth Syst. Sci. 18 (2), 575–594.
Lundquist, J., Hughes, M., Gutmann, E., Kapnick, S., 2020. Our skill in modeling mountain rain and snow is bypassing the skill of our observational networks. Bull. Am. Meteorol. Soc. 100 (12), 2473–2490.
Malguzzi, P., Grossi, G., Buzzi, A., Ranzi, R., Buizza, R., 2006. The 1966 "century" flood in Italy: a meteorological and hydrological revisitation. J. Geophys. Res. Atmos. 111 (D24).
Manzato, A., Davolio, S., Miglietta, M.M., Pucillo, A., Setvák, M., 2015. 12 September 2012: a supercell outbreak in NE Italy? Atmos. Res. 153, 98–118.
Mellor, G.L., Yamada, T., 1982. Development of a turbulence closure model for geophysical fluid problems. Rev. Geophys. 20, 851–875.
Mohr, S., Ehret, U., Kunz, M., Ludwig, P., Caldas-Alvarez, A., Daniell, J.E., Wisotzky, C., 2022. A multi-disciplinary analysis of the exceptional flood event of July 2021 in central Europe. Part 1: event description and analysis. Nat. Hazards Earth Syst. Sci. Discus. 2022, 1–44.
Molod, A., Takacs, L., Suarez, M., Bacmeister, J., 2015. Development of the GEOS-5 atmospheric general circulation model: evolution from MERRA to MERRA2. Geosci. Model Dev. 8 (5), 1339–1356.
Molteni, F., Buizza, R., Palmer, T.N., Petroliagis, T., 1996. The ECMWF ensemble prediction system: methodology and validation. Q. J. R. Meteorol. Soc. 122 (529), 73–119.
Morcrette, J., Barker, H.W., Cole, J., et al., 2008. Impact of a new radiation package, McRad, in the ECMWF integrated forecasting system. Mon. Weather Rev. 136 (12), 4773–4798.
Müller, S.K., Caillaud, C., Chan, S., De Vries, H., Bastin, S., Berthou, S., Warrach-Sagi, K., 2023. Evaluation of Alpine-Mediterranean precipitation events in convection-permitting regional climate models using a set of tracking algorithms. Clim. Dyn. 61 (1), 939–957.
Napoli, A., Crespi, A., Ragone, F., Maugeri, M., Pasquero, C., 2019. Variability of orographic enhancement of precipitation in the Alpine region. Sci. Rep. 9 (1), 13352.
Niu, G.Y., Yang, Z.L., Mitchell, K.E., Chen, F., Ek, M.B., Barlage, M., Xia, Y., 2011. The community Noah land surface model with multiparameterization options (Noah-MP): 1. Model description and evaluation with local-scale measurements. J. Geophys. Res. Atmos. 116 (D12).
Nkiaka, E., Nawaz, N.R., Lovett, J.C., 2017. Evaluating global reanalysis datasets as input for hydrological modelling in the Sudano-Sahel region. Hydrology 4 (1), 13.
Pal, S., Chang, H.I., Castro, C.L., Dominguez, F., 2019. Credibility of convection-permitting modeling to improve seasonal precipitation forecasting in the southwestern United States. Front. Earth Sci. 7, 11.
Pavan, V., Sannino, G., Vecchi, A., Volta, A., Antolini, G., Tesini, M.S., Giorgione, V., Cesari, D., Minguzzi, E., Giordani, A., Cerenzia, I., Selvini, A., Lo Monaco, A., Mallegni, R., Alessandrini, C., 2024. Atlante Eolico Emilia-Romagna Edizione 2024. Osservatorio Clima, Struttura IdroMeteoClima. ARPAE. https://www.arpae.it/it/temi-ambientali/clima/rapporti-e-documenti/atlante-eolico/atlante-eolico-2024.pdf [Accessed 2nd July 2025].
Pichelli, E., Coppola, E., Sobolowski, S., Ban, N., Giorgi, F., Stocchi, P., Vergara-Temprado, J., 2021. The first multi-model ensemble of regional climate simulations at kilometer-scale resolution Part 2: historical and future simulations of precipitation. Clim. Dyn. 56, 3581–3602.
Prein, A.F., Gobiet, A., 2017. Impacts of uncertainties in European gridded precipitation observations on regional climate analysis. Int. J. Climatol. 37 (1), 305.
Prein, A.F., Gobiet, A., Suklitsch, M., Truhetz, H., Awan, N.K., Keuler, K., Georgievski, G., 2013a. Added value of convection permitting seasonal simulations. Clim. Dyn. 41, 2655–2677.
Prein, A.F., Holland, G.J., Rasmussen, R.M., Done, J., Ikeda, K., Clark, M.P., Liu, C.H., 2013b. Importance of regional climate model grid spacing for the simulation of heavy precipitation in the Colorado headwaters. J. Clim. 26 (13), 4848–4857.
Prein, A.F., Langhans, W., Fosser, G., Ferrone, A., Ban, N., Goergen, K., Leung, R., 2015. A review on regional convection-permitting climate modeling: demonstrations, prospects, and challenges. Rev. Geophys. 53 (2), 323–361.
Prein, A.F., Ban, N., Ou, T., Tang, J., Sakaguchi, K., Collier, E., Chen, D., 2023. Towards ensemble-based kilometer-scale climate simulations over the third pole region. Clim. Dyn. 60 (11), 4055–4081.
Raffa, M., Reder, A., Marras, G.F., Mancini, M., Scipione, G., Santini, M., Mercogliano, P., 2021. VHR-REA_IT dataset: very high resolution dynamical downscaling of ERA5 reanalysis over Italy by COSMO-CLM. Data 6 (8), 88.
Rasmussen, R.M., Chen, F., Liu, C.H., Ikeda, K., Prein, A., Kim, J., Miguez-Macho, G., 2023. CONUS404: the NCAR–USGS 4-km long-term regional hydroclimate reanalysis over the CONUS. Bull. Am. Meteorol. Soc. 104 (8), E1382–E1408.
Raut, B.A., Jackson, R., Picel, M., Collis, S.M., Bergemann, M., Jakob, C., 2021. An adaptive tracking algorithm for convection in simulated and remote sensing data. J. Appl. Meteorol. Climatol. 60 (4), 513–526.
Regione Marche, 2013. Dipartimento per le Politiche Integrate di Sicurezza e per la Protezione Civile, Centro Funzionale per la Meteorologia, l'Idrologia e la Sismologia. Rapporto di evento 10–13 novembre 2013, Technical report. https://www.regione.marche.it/Portals/0/Protezione_Civile/Manuali%20e%20Studi/Rapporto_Evento_2013_11_30.pdf?ver=2016-04-19-121004-000.
Risanto, C.B., Moker Jr., J.M., Arellano Jr., A.F., Castro, C.L., Serra, Y.L., Luong, T.M., Adams, D.K., 2023. On the collective importance of model physics and data

assimilation on mesoscale convective system and precipitation forecasts over complex Terrain. Mon. Weather Rev. 151 (8), 1993–2008.
Ritter, B., Geleyn, J.F., 1992. A comprehensive radiation scheme for numerical weather prediction models with potential applications in climate simulations. Mon. Weather Rev. 120 (2), 303–325.
Rotunno, R., Ferretti, R., 2001. Mechanisms of intense Alpine rainfall. J. Atmos. Sci. 58 (13), 1732–1749.
Sahai, A.K., Kaur, M., Joseph, S., Dey, A., Phani, R., Mandal, R., Chattopadhyay, R., 2021. Multi-model multi-physics ensemble: a futuristic way to extended range prediction system. Front. Clim. 3, 655919.
Sangelantoni, L., Sobolowski, S., Lorenz, T., Hodnebrog, Ø., Cardoso, R.M., Soares, P.M. M., Bastin, S., 2023. Investigating the representation of heatwaves from an ensemble of km-scale regional climate simulations within CORDEX-FPS convection. Clim. Dyn. 1–37.
Schaefer, J.T., 1990. The critical success index as an indicator of warning skill. Weather Forecast. 5 (4), 570–575.
Schär, C., Ban, N., Fischer, E.M., Rajczak, J., Schmidli, J., Frei, C., Zwiers, F.W., 2016. Percentile indices for assessing changes in heavy precipitation events. Clim. Chang. 137, 201–216.
Schättler, U., Doms, G., Schraff, C., 2018. A description of the nonhydrostatic regional COSMO-model. In: Part VII: User's Guide, Deutscher Wetterdienst Rep. COSMO-Model, p. 195.
Scinocca, J.F., Kharin, V.V., Jiao, Y., Qian, M.W., Lazare, M., Solheim, L., Dugas, B., 2016. Coordinated global and regional climate modeling. J. Clim. 29 (1), 17–35.
Seneviratne, S., et al., 2021. Chapter 11: Weather and climate extreme events in a changing climate. Contribution of working group I to the sixth assessment report of the intergovernmental panel on climate change. In: Climate Change 2021: The Physical Science Basis. Cambridge University Press Cambridge, Cambridge, UK and New York, USA, pp. 1513–1766.
Shah, M.A.R., Renaud, F.G., Anderson, C.C., Wild, A., Domeneghetti, A., Polderman, A., Zixuan, W., 2020. A review of hydro-meteorological hazard, vulnerability, and risk assessment frameworks and indicators in the context of nature-based solutions. Int. J. Disast. Risk Reduct. 50, 101728.
Skamarock, W.C., Klemp, J.B., Dudhia, J., Gill, D.O., Barker, D.M., Duda, M.G., Powers, J.G., 2008. A description of the advanced research WRF version 3. NCAR Techn. Note 475, 113.
Soares, P.M.M., Miranda, P.M.A., Siebesma, A.P., Teixeira, J., 2004. An eddy-diffusivity/mass-flux parametrization for dry and shallow cumulus convection. Quart. J. Royal Meteorol. Soc. J. Atmosph. Sci. Appl. Meteorol. Phys. Oceanogr. 130 (604), 3365–3383.
Sperati, S., Alessandrini, S., D'Amico, F., Cheng, W., Rozoff, C.M., Bonanno, R., Vergata, M.A., 2024. A new Wind Atlas to support the expansion of the Italian wind power fleet. Wind Energy 27 (3), 298–316.
Stocchi, P., Davolio, S., 2023. MORE (Moloch Reanalysis) Request for a Special Project. ECMWF. https://www.ecmwf.int/sites/default/files/special_projects/2023/spitstocc-2023-request.pdf (Accessed 2nd July 2025).
Stocchi, P., Pichelli, E., Torres Alavez, J.A., Coppola, E., Giuliani, G., Giorgi, F., 2022. Non-hydrostatic Regcm4 (RegCM4-NH): Evaluation of precipitation statistics at the convection-permitting scale over different domains. Atmosphere 13 (6), 861.
Tarek, M., Brissette, F.P., Arsenault, R., 2020. Evaluation of the ERA5 reanalysis as a potential reference dataset for hydrological modelling over North America. Hydrol. Earth Syst. Sci. 24 (5), 2527–2544.
Taylor, K.E., 2001. Summarizing multiple aspects of model performance in a single diagram. J. Geophys. Res. Atmos. 106 (D7), 7183–7192.
Taylor, C.M., de Jeu, R.A., Guichard, F., Harris, P.P., Dorigo, W.A., 2012. Afternoon rain more likely over drier soils. Nature 489 (7416), 423–426.
Taylor, C.M., Birch, C.E., Parker, D.J., Dixon, N., Guichard, F., Nikulin, G., Lister, G.M., 2013. Modeling soil moisture-precipitation feedback in the Sahel: Importance of spatial scale versus convective parameterization. Geophys. Res. Lett. 40 (23), 6213–6218.
Tebaldi, C., Knutti, R., 2007. The use of the multi-model ensemble in probabilistic climate projections. Philos. Trans. R. Soc. A Math. Phys. Eng. Sci. 365 (1857), 2053–2075.
Teixeira, J., Stevens, B., Bretherton, C.S., Cederwall, R., Doyle, J.D., Golaz, J.C., Soares, P.M., 2008. Parameterization of the atmospheric boundary layer: a view from just above the inversion. Bull. Am. Meteorol. Soc. 89 (4), 453–458.
Thompson, G., Field, P.R., Rasmussen, R.M., Hall, W.D., 2008. Explicit forecasts of winter precipitation using an improved bulk microphysics scheme. Part II: implementation of a new snow parameterization. Mon. Weather Rev. 136 (12), 5095–5115.
Tiedtke, M., 1989. A comprehensive mass flux scheme for cumulus parameterization in large-scale models. Mon. Weather Rev. 117 (8), 1779–1800.
Torma, C., Giorgi, F., Coppola, E., 2015. Added value of regional climate modeling over areas characterized by complex terrain—precipitation over the Alps. J. Geophys. Res. Atmos. 120 (9), 3957–3972.
Valmassoi, A., Keller, J.D., Potthast, R., 2025. The plans for the 2km ICON-LAM reanalyses ICON-FORCE (Fine-scale Observation-based Reanalysis for Central Europe). In: Proceedings of the (CON/OSMO/LM/T ER Seminar) 2025 Mar 10-14, DWD Headquarters, Offenbach, Germany. https://doi.org/10.5676/DWD_pub/nwv/iccarus_2025 [Accessed 2nd July 2025].
Van Lipzig, N.P.V., Walle, J.V.D., Belušić, D., Berthou, S., Coppola, E., Demuzere, M., Thiery, W., 2023. Representation of precipitation and top-of-atmosphere radiation in a multi-model convection-permitting ensemble for the Lake Victoria Basin (East-Africa). Clim. Dyn. 60 (11), 4033–4054.
Viterbo, F., Sperati, S., Vitali, B., D'Amico, F., Cavalleri, F., Bonanno, R., Lacavalla, M., 2024. MERIDA HRES: a new high-resolution reanalysis dataset for Italy. Meteorol. Appl. 31 (6), e70011. https://doi.org/10.1002/met.70011.
Wahl, S., Bollmeyer, C., Crewell, S., Figura, C., Friederichs, P., Hense, A., Ohlwein, C., 2017. A novel convective-scale regional reanalysis COSMO-REA2: improving the representation of precipitation. Meteorol. Z. 26 (4), 345–361.
Weisman, M.L., Skamarock, W.C., Klemp, J.B., 1997. The resolution dependence of explicitly modeled convective systems. Mon. Weather Rev. 125 (4), 527–548.
Weusthoff, T., Ament, F., Arpagaus, M., Rotach, M.W., 2010. Assessing the benefits of convection-permitting models by neighborhood verification: examples from MAP D-PHASE. Mon. Weather Rev. 138 (9), 3418–3433.
Wouters, H., Demuzere, M., Blahak, U., Fortuniak, K., Maiheu, B., Camps, J., van Lipzig, N.P., 2016. The efficient urban canopy dependency parametrization (SURY) v1. 0 for atmospheric modelling: description and application with the COSMO-CLM model for a Belgian summer. Geosci. Model Dev. 9 (9), 3027–3054.
Wu, J., Lu, G., Wu, Z., 2014. Flood forecasts based on multi-model ensemble precipitation forecasting using a coupled atmospheric-hydrological modeling system. Nat. Hazards 74, 325–340.
Xu, Z., Chen, J., Jin, Z., Li, H., Chen, F., 2020. Assessment of the forecast skill of multiphysics and multistochastic methods within the GRAPES regional ensemble prediction system in the east Asian monsoon region. Weather Forecast. 35 (3), 1145–1171.
Ye, H., 2018. Changes in duration of dry and wet spells associated with air temperatures in Russia. Environ. Res. Lett. 13 (3), 034036.
Zampieri, M., Malguzzi, P., Buzzi, A., 2005. Sensitivity of quantitative precipitation forecasts to boundary layer parameterization: a flash flood case study in the Western Mediterranean. Nat. Hazards Earth Syst. Sci. 5 (4), 603–612.
Zittis, G., Bruggeman, A., Lelieveld, J., 2021. Revisiting future extreme precipitation trends in the Mediterranean. Weather Clim. Extrem. 34, 100380.
Zsótér, E., Pappenberger, F., Smith, P., Emerton, R.E., Dutra, E., Wetterhall, F., Balsamo, G., 2016. Building a multimodel flood prediction system with the TIGGE archive. J. Hydrometeorol. 17 (11), 2923–2940.